Spheroidal and conical shapes of ferrofluid-filled capsules in magnetic fields

Christian Wischnewski[*] and Jan Kierfeld[†]
Department of Physics, TU Dortmund University, 44221 Dortmund, Germany

(Received 20 October 2017; published 16 April 2018)

We investigate the deformation of soft spherical elastic capsules filled with a ferrofluid in external uniform magnetic fields at fixed volume by a combination of numerical and analytical approaches. We develop a numerical iterative solution strategy based on nonlinear elastic shape equations to calculate the stretched capsule shape numerically and a coupled finite element and boundary element method to solve the corresponding magnetostatic problem and employ analytical linear response theory, approximative energy minimization, and slender-body theory. The observed deformation behavior is qualitatively similar to the deformation of ferrofluid droplets in uniform magnetic fields. Homogeneous magnetic fields elongate the capsule and a discontinuous shape transition from a spheroidal shape to a conical shape takes place at a critical field strength. We investigate how capsule elasticity modifies this hysteretic shape transition. We show that conical capsule shapes are possible but involve diverging stretch factors at the tips, which gives rise to rupture for real capsule materials. In a slender-body approximation we find that the critical susceptibility above which conical shapes occur for ferrofluid capsules is the same as for droplets. At small fields capsules remain spheroidal and we characterize the deformation of spheroidal capsules both analytically and numerically. Finally, we determine whether wrinkling of a spheroidal capsule occurs during elongation in a magnetic field and how it modifies the stretching behavior. We find the nontrivial dependence between the extent of the wrinkled region and capsule elongation. Our results can be helpful in quantitatively determining capsule or ferrofluid material properties from magnetic deformation experiments. All results also apply to elastic capsules filled with a dielectric liquid in an external uniform electric field.

DOI: 10.1103/PhysRevFluids.3.043603

I. INTRODUCTION

Elastic capsules consist of a thin elastic shell enclosing a fluid inside. Elastic microcapsules are found in nature, for example, as red blood cells or virus capsids. They can also be produced artificially by various methods, for example, interfacial polymerization at liquid-liquid interfaces or multilayer polyelectrolyte deposition [1]. Artificially produced microcapsules are attractive systems for encapsulation and transport, for example, in delivery and release systems. Their overall shape is often nearly spherical and the shell can be treated as a two-dimensional elastic solid with a curved equilibrium shape. In experiments and for applications, elastic properties of capsules can be tuned by varying size, thickness, and shell materials. For applications involving delivery by rupture of capsules it is necessary to understand and characterize the mechanical properties and elastic instabilities of capsules.

The mechanical properties of elastic capsules are governed by the elastic shell, which is curved (typically spherical) in its equilibrium shape. This gives rise to different characteristic instabilities

[*]christian.wischnewski@tu-dortmund.de
[†]jan.kierfeld@tu-dortmund.de

in response to external forces [1–3]. Thin elastic membranes bend much more easily than stretch. This protects a curved equilibrium shape against deformations changing its Gaussian curvature and that is the reason for the stability of capsules under uniform compression. In contrast to fluid drops, elastic capsules under uniform compression fail in a buckling instability below a critical volume or critical internal pressure [4–9]. Buckling-type instabilities can also be triggered by external forces, for example, in electrostatically driven buckling transitions of charged shells [10] or in hydrodynamic flows [11]. Under point force loads, for example, exerted by atomic force microscopy tips, elastic capsules indent linearly at small forces and assume buckled shapes in the nonlinear regime at higher forces [2,12,13]. As opposed to fluid droplets, elastic capsules can also develop wrinkles upon deformation [14–17] if compressive hoop stresses arise.

Microcapsules can be manipulated and deformed in hydrodynamic flow [14,18,19], by micromanipulation using an atomic force microscope [2,3] or micropipettes or capillaries [16,17]. Another promising route to exert mechanical forces and to actuate elastic capsules in a noninvasive manner is via magnetic or electric fields [20,21]. For magnetic fields this requires the presence of magnetizable material either in the shell or in the capsule interior. The whole capsule then acquires a magnetic dipole moment, which can be manipulated in external magnetic fields. For actuation by electric fields the capsule has to contain polarizable dielectric material such that the capsule acquires an electrostatic dipole moment, which can be manipulated by an electric field. Homogeneous fields orient dipole moments but also induce capsule deformations, which increase the size of the dipole moment after orientation. Therefore, homogeneous fields always lead to stretching and elongation of the capsule. Inhomogeneous fields can also exert a net force on the capsule and induce directed motion at fixed magnetic dipole moment along the field gradient.

In the following we focus on spherical elastic capsules that are filled with a (quiescent) magnetic fluid and deformed in homogeneous external magnetic fields. As magnetic fluid we consider a ferrofluid, which is a liquid that is magnetizable by external magnetic fields because it consist of ferromagnetic or ferrimagnetic nanoparticles suspended in a carrier fluid. Because of the small particle size, ferrofluids are stable against phase separation and show superparamagnetic behavior [22]. Ferrofluids are used in technical and medical applications [23–25]. All our results also apply to elastic capsules filled with a (quiescent) dielectric fluid which are placed in a homogeneous external electric field.

The problem of ferrofluid droplets in uniform external magnetic fields has already been theoretically studied in the literature. Also, a spherical ferrofluid droplet is elongated in the direction of the magnetic field for increasing field strength; the resulting elongated shape was observed to be nearly spheroidal [26]. Bacri and Salin [27] used the assumption of a spheroidal shape for a quite precise approximation of the elongation by minimizing the total energy. Although the droplet is only elongated by the field, an abrupt shape transition is possible [27]: Beyond a threshold magnetic field strength the spheroidal droplet becomes unstable and elongates discontinuously into a shape with conical tips. The conical shape is stabilized by a positive feedback between shape and magnetic field distribution: A sharp tip gives rise to a diverging field strength at the tip, which in turn generates strong stretching forces stabilizing the sharp tip. The mechanism of forming sharp tips is reminiscent of the normal field instabilities (Rosensweig instabilities) of free planar ferrofluid surfaces in a perpendicular homogeneous magnetic field, which were first described by Cowley and Rosensweig [28] and later extended by a nonlinear stability analysis to study subsequent pattern formation [29].

The discontinuous shape transition to a conical shape exhibits hysteresis and only occurs above a critical susceptibility χ_c of the ferrofluid. In Refs. [30,31] a value $\chi_c \simeq 16.59$ was found below which no conical shape can exist; a slender-body approximation in Ref. [32] gives $\chi_c \simeq 14.5$. Using the approximative energy minimization for spheroidal shapes of Bacri and Salin [27] gives $\chi_c \simeq 19.8$. The jump in droplet elongation at the transition to a conical shape depends on the magnetic susceptibility: Large elongation jumps are possible for high susceptibilities. This behavior was investigated in more detail in several numerical studies [33–35]. Apart from free ferrofluid droplets, the deformation behavior of sessile droplets on a plate [36] or sedimenting ferrofluid drops in external fields [37] have also been investigated for homogeneous external magnetic fields.

Dielectric droplets in a homogeneous external electric field exhibit the same shape transition from a spheroidal to a conical shape. For the electric field, however, free charges exist, and conducting droplets are easily realized experimentally. In fact, the first experimental observations of conical droplet shapes were made for water droplets [38] and soap bubbles [39]. In Ref. [31] it was shown that also a conducting liquid droplet surrounded by an outer conducting liquid in a homogeneous electric field exhibits conical shapes above a corresponding critical conductivity ratio $\sigma/\sigma_{\text{out}} = 1 + \chi_c \simeq 17.59$. In the limit of an ideally conducting droplet with infinite susceptibility or infinite conductivity (both resulting in zero electric field inside the droplet), the conical solutions in Refs. [30–32] approach Taylor's cone solution with a half opening angle $\simeq 49.3^\circ$ [40]. Both for liquid metal (i.e., ideally conducting) and dielectric droplets, the conic cusp formation has been studied dynamically and dynamic self-similar solutions have been obtained [41,42]. Fluid droplets, which are neither perfect conductors nor perfect insulators, disintegrate at higher external electric fields by emitting jets of fluid at the tip, from which small droplets pinch off. Also for this process, scaling laws for droplet sizes could be theoretically obtained [43,44].

In a ferrofluid-filled elastic capsule the ferrofluid drop is enclosed by a thin elastic membrane, which will modify the transition from a spheroidal to a conical shape observed for droplets. Such ferrofluid-filled capsules have already been realized experimentally. Neveu-Prin *et al.* [45] encapsulated ferrofluids by polymerization and analyzed the magnetization behavior of the magnetic capsules. Degen *et al.* [20] investigated experimentally elastic capsules filled with a magnetic liquid in an external magnetic field. They used a magnetic liquid consisting of micrometer-sized magnetic particles that do not show the special properties of ferrofluids but form long chains in the presence of external magnetic fields. These magnetite-filled elastic capsules could be actuated to deform in a magnetic field. A quantitative theoretical description of their deformation is still missing. In Ref. [21], capsules filled with a dielectric liquid in an external electric field were investigated experimentally and theoretically with a focus on small deformations.

We will describe the elastic shell by a nonlinear elastic model based on a Hookean elastic energy density for thin shells, assume axisymmetric capsules, and calculate the shape at force equilibrium by solving shape equations as they have been derived in Refs. [7,17]. As stated above, homogeneous magnetic fields acting on ferrofluid-filled capsules give rise to stretching and elongation of the capsule in order to increase the total dipole moment. Therefore, stretching tensions are dominant in the elastic shell. This is why we will consider the limiting case of vanishing bending modulus and bending moments for most of the present work, which is commonly called the elastic membrane limit (as opposed to the elastic shell case).

In our numerical approach, the magnetic field inside the capsule is calculated using a coupled finite element and boundary element method. The capsule shape provides the geometric boundary for the field calculation. Vice versa, the magnetic field distribution couples to the shape equations via the magnetic surface stresses. We solve the full coupled problem numerically by an iterative method.

We combine this numerical approach with several analytical approaches to investigate the capsule deformation in a homogeneous magnetic field as a function of the magnetic field strength and Young modulus of the capsule material. First we characterize the linear deformation regime of spheroidal capsules for small fields both numerically and analytically. Then we answer the question to what extent the elastic shell will suppress the discontinuous spheroidal to conical shape transition of a ferrofluid droplet and whether elastic properties such as the Young modulus of the shell material can be used to tune and control the instability. We show that conical shapes can also occur for capsules with nonlinear Hookean membranes but require diverging strains at the conical tips. As a real elastic material is not able to support arbitrarily high strains, we expect that diverging local stretch factors at the capsule poles indicate that real capsules tend to rupture close to the poles as soon as the conical shape is assumed. Then the existence of a sharp discontinuous shape transition into a conical shape provides an interesting route to trigger capsule rupture at the poles at rather well-defined magnetic (for ferrofluid-filled capsules) or electric (for dielectric-filled capsules) field values. The subsequent rupture process has some analogies to the onset of the disintegration of droplets in electric fields

[43,44], but our static approaches based on nonlinear Hookean material laws are not suited to model the rupture process itself.

We find that the discontinuous shape transition between spheroidal and conical shapes with hysteresis effects and shape bistability is also present for elastic ferrofluid-filled capsules. Numerically, we obtain a complete classification of the shape transition in the parameter plane of dimensionless magnetic field strengths (magnetic Bond number) and the dimensionless ratio of the Young modulus of the shell material and the surface tension of the ferrofluid. These findings are partly corroborated by an analytical approximative energy minimization extending the spheroidal shape approximation of Bacri and Salin [27] to ferrofluid-filled capsules. For conical shapes we generalize the slender-body approximations of Stone *et al.* [32], which allows us to quantify the divergence of local stretch factors at the capsule poles and to show that the same analytic formula as for ferrofluid droplets governs the dependence of the cone angle on the magnetic susceptibility χ (or the dielectric susceptibility $\varepsilon/\varepsilon_{\text{out}} - 1$ for a dielectric droplet with dielectric constant ε in a surrounding liquid with ε_{out}). In particular, we predict the critical susceptibility χ_c, above which the hysteretic shape transition between spheroidal and conical capsule shapes can be observed, to be *identical* to the critical value for ferrofluid or dielectric droplets. We also find that, for elastic capsules, magnetic stretching can give rise to wrinkling along the capsule equator region. We predict the parameter range for the appearance of wrinkles and the extent of the wrinkled region on a spheroidal capsule depending on its elastic properties and its elongation.

II. THEORETICAL MODEL AND NUMERICAL METHODS

We start with a ferrofluid drop suspended in an external nonmagnetic liquid of the same density as the ferrofluid, which eliminates gravitational forces. Thus the drop is force-free except for the surface tension γ, which forces the drop to be spherical and is balanced by internal pressure. If the drop is enclosed by an elastic shell, for example, after a polymerization reaction at the liquid-liquid interface, we have a spherical elastic capsule. We assume that the relaxed rest shape of this capsule is spherical with a rest radius R_0, which is given by the fixed volume $V_0 = 4\pi R_0^3/3$ of the droplet or capsule.

After applying a uniform magnetic field $H_0\mathbf{e}_z$ in the z direction, the resulting shape of the capsule becomes stretched in the z direction, but the capsule shape and magnetic field distribution remain axisymmetric around the z axis. A uniform external magnetic field causes mirror-symmetric forces on the capsule, resulting in a shape with reflection symmetry with respect to the plane $z = 0$ (see Fig. 1).

A. Geometry

We describe the axisymmetric shell using cylindrical coordinates r, z, and φ. The capsule's shell is thin compared to its diameter, so we consider the shell to be a two-dimensional elastic surface. Because of the axial symmetry, we only need the contour line $r(z)$ to describe the whole capsule shape.

For our calculations, we parametrize the surface by the arc length s_0 of the undeformed spherical contour with $s_0 \in [0, L_0 = \pi R_0]$, starting at the lower apex and ending at the upper apex. Using the reflection symmetry, we only need half of that interval, $s_0 \in [0, L_0/2]$, to describe the capsule's shape completely. In addition to the coordinates $r(s_0)$ and $z(s_0)$, we define a slope angle $\psi(s_0)$ by the unit vector $\mathbf{e}_s$ following the contour line via $\mathbf{e}_s = (\cos\psi, \sin\psi)$.

B. Magnetostatics

1. Forces by the ferrofluid

In order to calculate the shape of the capsule in an external magnetic field, we have to take the magnetic forces that are caused by the ferrofluid on the capsule surface into account. Because we

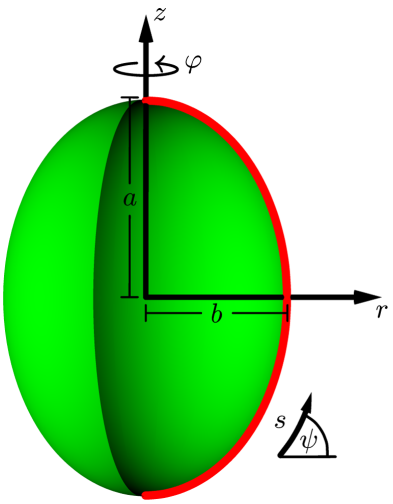

FIG. 1. Illustration of the parametrization in cylindrical coordinates (r,z,φ) and the contour line with arc length s. The complete capsule is obtained by revolution of the red contour line, while the angle ψ describes its slope. This contour line is calculated numerically. The polar radius is called a, while b denotes the equatorial radius.

are interested in a static solution, we can assume that the fluid is at rest. Then the fluid can only exert hydrostatic forces *normal* to the surface, while tangential components are zero. In order to calculate the normal magnetic force density $f_m(r,z)$ on the surface, we use the magnetic stress tensor by Rosensweig [22],

$$f_m(r,z) = \mu_0 \int_0^{H(r,z)} M(r,z) dH(r,z) + \frac{\mu_0}{2} M_n^2(r,z). \tag{1}$$

Here $M = |\mathbf{M}|$ is the absolute value of the magnetization and $M_n = \mathbf{M} \cdot \mathbf{n}$ its normal component ($\mathbf{n}$ is the outward unit normal to the capsule surface). Magnetization M and magnetic field H are taken on the inside of the capsule surface.

We assume a linear magnetization law

$$\mathbf{M} = \chi \mathbf{H} \tag{2}$$

with a susceptibility χ for the ferrofluid ($\chi = \mu - 1$ in terms of its magnetic permeability μ), which is justified for small fields $H \ll M_s/3\chi$, where M_s is the saturation magnetization of the ferrofluid. References [46,47] studied the behavior of drops with a nonlinear Langevin magnetization (polarization) law. The saturation of the magnetization or polarization forbids sharp tips and leads to more rounded drops. It was shown, on the other hand, that the linear law is a very good approximation for small and even medium fields. This typically requires the maximum magnetic flux density $B_{\max} = \mu_0 H_{\max}$ to be in a range of 50–100 mT, depending on the specific fluid [36,48]. For a linear magnetization we can rewrite Eq. (1) as

$$f_m(r,z) = \frac{\mu_0 \chi}{2} \left[H^2(r,z) + \chi H_n^2(r,z) \right] \tag{3}$$

(assuming $\chi_{\text{out}} = 0$ for the external nonmagnetic liquid or using $\chi = \mu/\mu_{\text{out}} - 1$ in terms of the magnetic permeabilities μ of the ferrofluid and the μ_{out} of the external liquid), where $H = |\mathbf{H}|$ and H_n is the normal component of the magnetic field. We will use this position-dependent normal magnetic force density to modify the pressure in our elastic equations in Sec. II C 1.

2. Calculation of the magnetic field

To calculate the total magnetic field, i.e., the superposition of the external uniform field and the field from the ferrofluid magnetization, we use the fact that ferrofluids are generally nonconducting [22]. Then Maxwell's equations give $\nabla \times \mathbf{H} = 0$, which allows us to introduce a scalar magnetic potential u with $\nabla u = \mathbf{H}$. From Maxwell's equation $\nabla \cdot \mathbf{B} = \nabla \cdot \mu_0(\mathbf{H} + \mathbf{M}) = 0$ we get Poisson's equation in magnetostatics

$$\nabla^2 u(r,z) = -\nabla \cdot \mathbf{M}(r,z). \tag{4}$$

For the linear magnetization law (2), Poisson's equation simplifies to the Laplace equation $\nabla^2 u(r,z) = 0$.

For the numerical solution of this partial differential equation we use a coupled axisymmetric finite element–boundary element method [49–52] with a cubic spline interpolation for the boundary [53]. This combination of methods was also used by Lavrova *et al.* for free ferrofluid drops [34,54,55] and earlier for electric drops, e.g., by Harris and Basaran [56]. The finite element method (FEM) is used to solve Eq. (4) in the magnetized domain inside the capsule and the boundary element method (BEM) for the nonmagnetic domain outside. Both domains are coupled by the continuity conditions of magnetostatics for u and its normal derivative on the boundary of the capsule,

$$u_{\text{in}} = u_{\text{out}}, \quad \mu \frac{\partial u_{\text{in}}}{\partial n} = \frac{\partial u_{\text{out}}}{\partial n}, \tag{5}$$

with $\mu_{\text{out}} = 1$ for the external nonmagnetic liquid. Both the FEM and BEM exploit axial symmetry and effectively operate in the two-dimensional rz plane, where the axisymmetric capsule shape is described by a contour line $(r(s),z(s))$. For the FEM we use a standard Galerkin method with linear elements on a triangular two-dimensional grid in the rz plane that is created with a Delauney triangulation using the Fade2D software package [57], where we set a fixed number of grid points on the capsule's boundary.

In the BEM we express solutions $u(\mathbf{r}_0)$ of the Laplace equation $\nabla^2 u = 0$ for $\mathbf{r}_0$ on the outside or the boundary of the capsule in terms of integrals over the boundary of the capsule. Using fundamental solutions with rotational symmetry [58], we have to solve a set of one-dimensional integrals over the whole boundary of the capsule

$$c u(\mathbf{r}_0) - \int_0^L \left[u(\mathbf{r}) \frac{\partial u^*_{\text{ax}}(\mathbf{r}_0,\mathbf{r})}{\partial n} - \frac{\partial u(\mathbf{r})}{\partial n} u^*_{\text{ax}}(\mathbf{r}_0,\mathbf{r}) \right] r \, ds = z_0. \tag{6}$$

Here $u^*_{\text{ax}}(\mathbf{r}_0,\mathbf{r}) \equiv \int_0^{2\pi} u^*(\mathbf{r}_0,\mathbf{r}) d\varphi$ is the axially symmetric fundamental solution of Laplace's equation, which is obtained from the fundamental solution $u^*(\mathbf{r},\mathbf{r}_0) = 1/4\pi|\mathbf{r} - \mathbf{r}_0|$ of Laplace's equation, $\Delta u^*(\mathbf{r},\mathbf{r}_0) = -\delta(\mathbf{r} - \mathbf{r}_0)$. In the integral equation (6), u and its normal derivative are evaluated on the outside of the capsule surface. The point $\mathbf{r}_0$ is the point where u is to be calculated, while the integrals are taken over points $\mathbf{r}(s)$ on the capsule contour. Both $\mathbf{r}$ and $\mathbf{r}_0$ lie in the same rz plane. For the geometric factor c, we have $c = 1/2$ for points $\mathbf{r}_0$ on the boundary Γ and $c = 1$ for points $\mathbf{r}_0$ in the exterior domain. The vector $\mathbf{n}$ denotes the outward unit normal vector and z_0 describes the z component of $\mathbf{r}_0$. On the right-hand side of (6), z_0 can be interpreted as the potential of the external electric field. For numerical evaluation, the integrals in Eq. (6) are discretized by a point collocation method and solved by applying Gaussian quadrature for nonsingular integrands and a midpoint rule for weakly singular integrands.

The FEM and BEM are coupled at the boundary by the continuity conditions (5). The FEM provides values for u on every finite element grid point inside the capsule including values u_{in} on the inner side of the boundary; in addition, the normal derivatives $\partial u_{\text{in}}/\partial n$ on the inside of the discretized capsule boundary are needed for the FEM but remain *a priori* unknown. Values for these normal derivatives on the boundary points of the FEM grid are obtained by the BEM method. Our BEM uses linear interpolation for u between the discretized boundary points. We use the continuity conditions (5) to write the boundary integral equation (6) in terms of quantities on the inner capsule boundary.

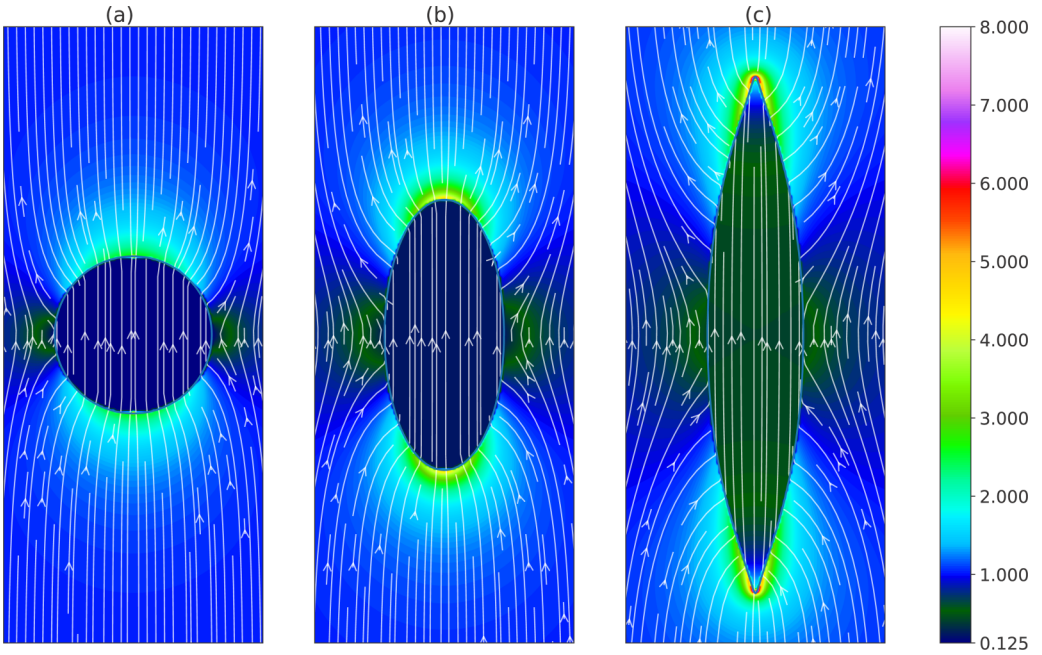

FIG. 2. Numerical results for the magnetic field distribution and capsule shape (two-dimensional projection) for a capsule filled with a ferrofluid with a susceptibility of $\chi = 21$. The ratio of Young's modulus and surface tension is $Y_{2D}/\gamma = 100$. The external magnetic field H_0 is uniform and points in the upward direction. Arrows indicate the local direction of H; the color codes for the absolute value of H in units of H_0. The (a) spherical capsule and (b) spheroidal capsule have uniform fields inside, while the field in the (c) conical-shaped capsule increases strongly in the tips. The elongations a/b (ratio of the polar radius to the equatorial radius) are (a) $a/b = 1$, (b) $a/b = 2.26$, and (c) $a/b = 5.38$. The magnetic Bond numbers B_m [see the definition in Eq. (23)] are (a) $B_m = 0$, (b) $B_m = 262.4$, and (c) $B_m = 702.2$.

Using one BEM equation (6) for each boundary point (with $c = 1/2$), we obtain a set of equations that allows us to calculate the unknown derivatives $\partial u_{\text{in}}/\partial n$ for given u_{in} and to get a closed system of equations for u everywhere inside the capsule. After solving the resulting system of FEM equations, we know u everywhere inside the capsule. For the calculation of u inside the capsule and thus for the calculation of the magnetic force density $f_m(r,z)$ acting on the capsule using (3), which is also calculated with the magnetic field on the inside, it is not necessary to calculate u in the entire external domain explicitly. This is done implicitly by the BEM. If needed (for example, in order to calculate the field in the exterior regions in Fig. 2), u can be calculated by solving (6) for points $\mathbf{r}_0$ in the exterior with $c = 1$.

In a ferrofluid capsule or drop with sharp edges, very high field strengths can arise [see Fig. 2(c)]. Also field gradients can be large, which makes pointed shapes prone to discretization errors caused by the grid. This effect can be countered to some degree by placing more FEM grid points at the tip in order to improve the precision there, which is, however, limited by the BEM part of the solution scheme: The collocation points must not come too close to the symmetry axis because the weakly singular integrals become strongly singular on the z axis [59]. This leads to massively increasing numerical errors near the axis and a decrease of the overall precision. Overall, our numerical scheme to calculate singular BEM integrals is not the most advanced as a trade-off for simplicity. There are more elaborated schemes for the integration of singular integrals as, for example, developed over many years by Gray *et al.* [60,61], which could provide a more elegant way to deal with the problem. We use the following compromise for the discretization: We place $N = 250$ elements on the boundary such that the length L_i of the ith boundary element (beginning at the equator) is

given by

$$L_i = c_0 \exp\left(\ln(l_0)\frac{i-1}{N}\right). \tag{7}$$

The constant c_0 is chosen in order to obtain the correct total arc length L, which is given by the meridional stretch factors $\lambda_s = ds/ds_0$ of the deformed capsule [see Eq. (11) below], $\sum_{i=1}^{N} L_i = L/2 = \int_0^{L_0/2} \lambda_s ds_0$. We choose $l_0 = 0.1$ ($l_0 = 1$ gives a constant element length and $l_0 < 1$ leads to a higher element density at the capsule's tip). Increasing N beyond 250 does not improve the precision significantly. A higher density of points at the capsule's tip (lower l_0) leads to stronger oscillations in the iterative solution scheme (see Sec. II D below).

3. Electric fields and dielectric liquid

Our approach to elastic capsules filled with a ferrofluid in a magnetic field also applies to capsules filled with a dielectric fluid in an electric field. The generic situation for a capsule filled with a fluid with dielectric constant ε is to be suspended in a dielectric liquid with a different $\varepsilon_{\text{out}} \neq \varepsilon$, which does not equal unity $\varepsilon_{\text{out}} \neq 1$. Then the dielectric force density in a linear medium is

$$f_e(r,z) = \frac{\varepsilon_0 \varepsilon_{\text{out}} \chi_\varepsilon}{2}\left(E^2(r,z) + \chi_\varepsilon E_n^2(r,z)\right), \quad \chi_\varepsilon \equiv \frac{\varepsilon}{\varepsilon_{\text{out}}} - 1, \tag{8}$$

which is completely analogous to (3) with χ_ε playing the role of the susceptibility χ. For the general case, Poisson's equation becomes

$$\nabla^2 \phi(r,z) = -\frac{1}{\epsilon_0} \nabla \cdot \mathbf{P}(r,z), \tag{9}$$

with the electric potential ϕ and the polarization $\mathbf{P}$. For a linear polarization law, it simplifies to the Laplace equation $\nabla^2 \phi(r,z) = 0$.

C. Equilibrium shape of the capsule

1. Elasticity and shape equations

The capsule is deformed by the normal magnetic stresses f_m from the ferrofluid. We have to calculate the resulting deformed equilibrium shape, where all elastic stresses, surface tension, and magnetic stress are balanced everywhere on the capsule. Every point of the reference shape $[r_0(s_0), z_0(s_0)]$ is mapped onto a new point $[r(s_0), z(s_0)]$. The deformed shape $[r(s_0), z(s_0)]$ is calculated by solving shape equations, which are derived from nonlinear theory of thin shells [7,17,62,63]. We use a Hookean elastic energy density with a spherical rest shape. The Hookean elastic energy density (defined as energy per undeformed unit area) is given by

$$w_s = \frac{1}{2}\frac{Y_{2\text{D}}}{1-\nu^2}\left(e_s^2 + 2\nu e_s e_\varphi + e_\varphi^2\right) + \frac{1}{2} E_{\text{B}}\left(K_s^2 + 2\nu K_s K_\varphi + K_\varphi^2\right). \tag{10}$$

Here e_s and e_φ are meridional and circumferential strains that contain the stretch factors λ_s and λ_φ:

$$e_s = \lambda_s - 1, \quad e_\varphi = \lambda_\varphi - 1, \quad \lambda_s = \frac{ds}{ds_0}, \quad \lambda_\varphi = \frac{r}{r_0}. \tag{11}$$

Here and in the following, quantities with subscript 0 refer to the undeformed spherical reference shape and quantities without 0 describe the deformed shape. Analogously, the bending strains K_s and K_φ are generated by the curvatures κ_s and κ_φ:

$$K_s = \lambda_s \kappa_s - \kappa_{s0}, \quad K_\varphi = \lambda_\varphi \kappa_\varphi - \kappa_{\varphi 0}, \quad \kappa_s = \frac{d\psi}{ds}, \quad \kappa_\varphi = \frac{\sin\psi}{r}.$$

In the elastic energy (10), $Y_{2\text{D}}$ is the two-dimensional Young modulus governing stretching deformations, E_{B} is the bending modulus, and ν is the two-dimensional Poisson ratio. Elastic

properties are usually only weakly ν dependent; we use $\nu = 1/2$, which is the typical value for an incompressible polymeric material. The arc length of the deformed capsule's contour is given by $L = \int_0^{L_0} \lambda_s ds_0$, while $L_0 = \pi R_0$ is the fixed arc length of the undeformed spherical capsule.

In experiments, the capsule's shell is constructed by polymerization on the surface of a drop. Therefore, the undeformed reference shape, which is spherical in the absence of gravity, is also a solution of the Laplace-Young equation

$$\gamma(\kappa_s + \kappa_\varphi) = p, \tag{12}$$

where γ is the surface tension of the droplet. The solution of the Laplace-Young equation will be discussed in detail in Sec. II C 4 below.

In the following we will neglect the bending energy, which means we set $E_B = 0$. The characteristic length scale of the problem is the radius R_0 of the undeformed sphere such that the neglect of the bending energy corresponds to the limit of large Föppl–von Kármán numbers $\gamma_{\mathrm{FvK}} \equiv Y_{2D} R_0^2 / E_B$. This is the limiting case of an elastic Hookean membrane and is a good approximation for two reasons. First, we will only consider capsules with thin shells as they were prepared in experiments [17,20]. The shell thickness D is very small compared to the capsule size, $D \ll R_0$. With $Y_{2D} \propto D$ and $E_B \propto D^3$ it follows that $\gamma_{\mathrm{FvK}} \sim (R_0/D)^2 \gg 1$ and stretching energies are typically larger than bending energies. The second argument is that the homogeneous magnetic field acting on the ferrofluid-fluid capsule predominantly stretches and elongates the capsule in order to increase its total dipole moment. This increases stretching energies, whereas the capsules develop high curvatures only at the conical tips. However, we show below that stretch factors diverge at conical tips, so the stretching energy dominates over the bending energy associated with these high curvatures also in the tip regions.

Elastic tensions in the shell (defined as force per deformed unit length) derive from the surface elastic energy density by

$$\begin{aligned} \tau_s &= \frac{1}{\lambda_\varphi} \frac{\partial w_s}{\partial e_s} = \frac{Y_{2D}}{(1-\nu^2)\lambda_\varphi} [(\lambda_s - 1) + \nu(\lambda_\varphi - 1)], \\ \tau_\varphi &= \frac{1}{\lambda_s} \frac{\partial w_s}{\partial e_\varphi} = \frac{Y_{2D}}{(1-\nu^2)\lambda_s} [(\lambda_\varphi - 1) + \nu(\lambda_s - 1)]. \end{aligned} \tag{13}$$

Although we use a Hookean elastic energy density, the constitutive relation (13) is *nonlinear* because of the additional $1/\lambda$ factors, which arise for purely geometrical reasons: The Hookean elastic energy density is defined per undeformed unit area such that $\partial w_s / \partial e_s$ is the force per undeformed unit length, whereas the Cauchy stresses τ_s and τ_φ are defined per deformed unit length.

In addition to the elastic tensions τ_s and τ_φ, there is also a contribution from an isotropic effective surface tension γ between the outer liquid and the capsule. Such a contribution arises either as the sum of surface tensions of the liquid outside with the outer capsule surface and the liquid inside with the inner capsule surface or, if the capsule shell is porous such that there is still contact between the liquids outside and inside the capsule, with additional contributions from the surface tension between outside and inside liquids. In the absence of elastic tensions, the surface tension γ also gives rise to the spherical rest shape of the capsule. For macroscopic capsules the surface tensions should be negligible, but for microcapsules with weak walls they should not be neglected. We expect the effective surface tension γ to be somewhat smaller than typical liquid-liquid surface tensions, which are around $\gamma = 50$ mN/m; we will use $\gamma = 10$ mN/m below.

The equilibrium of forces in the deformed elastic membrane is described by

$$0 = \tau_s \kappa_s + \tau_\varphi \kappa_\varphi + (\kappa_s + \kappa_\varphi)\gamma - p, \tag{14}$$

$$0 = \frac{\cos\psi}{r} \tau_\varphi - \frac{1}{r} \frac{d(r\tau_s)}{ds}, \tag{15}$$

where Eq. (14) describes the normal force equilibrium and Eq. (15) tangential force equilibrium (in the s direction, equilibrium in the φ direction is always fulfilled by axial symmetry). In the presence of magnetic forces, the pressure

$$p(s) = p_0 + f_m(s) \tag{16}$$

is modified by the magnetic stress f_m, which is a position-dependent normal stress pointing outwards and thus stretching the capsule and given by the magnetic field at the capsule surface [see Eq. (3)]. It is important to note that magnetic forces are always normal to the surface such that they do no enter the tangential force equilibrium (15). The (homogeneous) pressure p_0 is the Lagrange multiplier for the volume constraint $V = V_0 = 4\pi R_0^3/3$.

The equations of force equilibrium and geometric relations can be used to derive a system of four first-order differential equations with the arc length s_0 of the undeformed spherical contour as an independent variable, which are called shape equations in the following:

$$\begin{aligned} r'(s_0) &= \lambda_s \cos\psi, \quad z'(s_0) = \lambda_s \sin\psi, \\ \psi'(s_0) &= \frac{\lambda_s}{\tau_s + \gamma}[-\kappa_\varphi(\tau_\varphi + \gamma) + p(s_0)], \\ \tau_s'(s_0) &= \lambda_s \frac{\cos\psi}{r}(\tau_\varphi - \tau_s). \end{aligned} \tag{17}$$

In these shape equations, the surface tension γ gives an isotropic and constant stress contribution, in addition to the elastic stresses τ_s and τ_φ. This is because we assume that the undeformed rest state, where the elastic stresses τ_s and τ_φ vanish, is identical to the shape of a ferrofluid droplet of surface tension γ. We neglect that γ could change during capsule preparation and during elastic deformation.

The system of shape equations is closed by the constitutive relation (13) for τ_φ and the relations

$$\lambda_s = (1-\nu^2)\lambda_\varphi \frac{\tau_s}{Y_{2D}} - \nu(\lambda_\varphi - 1) + 1 \quad \text{with } \lambda_\varphi = \frac{r}{r_0}, \quad \kappa_\varphi = \frac{\sin\psi}{r},$$

where the first relation derives from the constitutive relation (13) for τ_s and the second relation is geometrical. For further details on the derivation of the shape equations, we refer the reader to Refs. [7,17,62].

2. Numerical solution of the shape equations

The system of shape equations (17) has to be solved numerically. The integration starts at the pole with $s_0 = 0$ and runs to the capsule's equator at $s_0 = L_0/2$. To integrate the four first-order differential equations we have three boundary conditions at $s_0 = 0$:

$$r(0) = 0, \quad z(0) \text{ arbitrary}, \quad \psi(0) = 0. \tag{18}$$

The condition for $r(0)$ follows from the absence of holes in the capsule. We can choose $z(0)$ arbitrarily because the external magnetic field does not depend on the z coordinate. The boundary condition $\psi(0) = 0$ at the pole seems to exclude possible conical capsule shapes with $\psi(0) > 0$. We discuss this issue below in Sec. III C and in Appendix C 3. There we derive the boundary condition $\psi(0) = 0$ for finite stretches λ_s and λ_φ at the poles. The boundary condition $\psi(0) = 0$ also arises if the magnetic forces f_m remain finite at the poles such that the normal force equilibrium requires finite curvatures at the poles. Conical shapes, however, have divergent stretches λ_s and λ_φ and divergent magnetic normal forces f_m at their conical tips. In the numerical calculation of capsule shape and magnetic field we have to discretize the capsule surface such that divergences are cut off (this numerical issue is discussed in more detail also in Appendix D) and the boundary condition $\psi(0) = 0$ for finite stretches λ_s and λ_φ or finite magnetic force f_m is appropriate. Then the right-hand side of the shape equation for τ_s in Eq. (17) vanishes, $\tau_s'(0) = 0$ for $s_0 = 0$ [see also Eq. (C14)], which can be used to start the integration at the pole. *A priori*, a fourth boundary condition for the tension $\tau_s(0)$ at the pole is unknown. On the other hand, we have $\psi(L_0/2) = \pi/2$ as a matching condition at $s_0 = L_0/2$

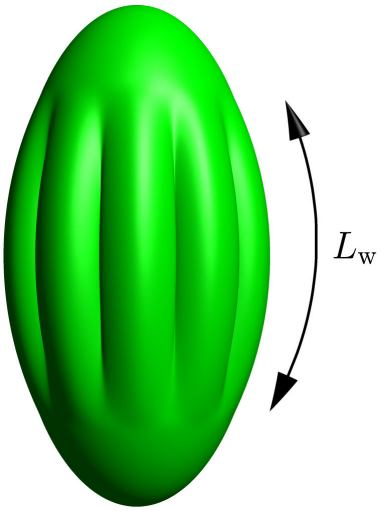

FIG. 3. Three-dimensional illustration of a wrinkled capsule. The length L_{w} of the wrinkles is measured as the length of the region, where $\tau_\varphi + \gamma < 0$. The wrinkling wavelength is not determined explicitly here.

to prevent kinks there. With the help of this matching condition, we can use a shooting method to determine $\tau_s(0)$. To increase numerical stability, we expand the shooting method to a multiple shooting method, where we use several integration intervals with several matching points.

To keep the volume of the capsule constant, we have to use the internal pressure p_0 as the Lagrange multiplier, which is adjusted during the calculation. In order to do so, p_0 becomes another shooting parameter with $V - V_0$ as the corresponding residual. In this work we use a fourth-order Runge-Kutta scheme with a step size of $\Delta s_0 = 10^{-6}$ in the first integration interval starting at the apex and $\Delta s_0 = 10^{-4}$ in all other intervals, while there is a total of 250 integration intervals.

3. Wrinkling

A ferrofluid-filled capsule is stretched in a uniform external magnetic field in the direction of the magnetic field. As opposed to a ferrofluid droplet, a capsule can develop wrinkles if circumferential compressive stresses arise as a result of this stretching.

Because of volume conservation, the circumferential radius of the capsule has to decrease in the equator region, giving rise to compression with $\lambda_\varphi < 1$ in this region, and a region of negative elastic stress $\tau_\varphi < 0$ develops. In contrast to a droplet with a liquid surface and constant surface tension $\gamma > 0$, regions of negative total hoop stress $\gamma + \tau_\varphi < 0$ can develop for capsules if the negative elastic hoop stress exceeds the surface tension. Then the elastic shell can reduce its total energy by developing wrinkles in the circumferential direction (see Fig. 3 for illustration). These wrinkles cost stretching energy in the meridional s direction and bending energy, but this is compensated by a release of compressional stresses and a reduction of elastic compression energy in the φ direction. Strictly speaking, $\gamma + \tau_\varphi < 0$ is only an approximation neglecting the bending energy, which will also increase upon wrinkling, and the negative stress has to exceed a small Euler-like threshold value. We expect the wrinkles to occur in a region near the capsule equator. Thus they will be roughly parallel to the external magnetic field and therefore we assume that they do not effect the magnetic properties of the capsule.

In order to introduce wrinkling in the shape equations, we will use the same approach that has been used for pendant capsules in Ref. [17]. The wrinkles will break the axial symmetry. In the wrinkled regions, where $\gamma + \tau_\varphi < 0$, we approximate the shape by an axisymmetric pseudomidsurface $(\overline{r}(s_0), \overline{z}(s_0))$ for which we use modified axisymmetric shape equations, where we set $\gamma + \tau_\varphi = 0$. This

condition states that the total circumferential hoop stress is completely relaxed by fully developed wrinkles [64]. This leads us to a new set of equations (see also Ref. [17]), which read

$$\overline{r}'(s_0) = \lambda_s \cos\overline{\psi}, \quad z'(s_0) = \lambda_s \sin\overline{\psi}, \quad \overline{\psi}'(s_0) = \frac{\lambda_s}{\overline{\tau}_s + \overline{\gamma}} p, \quad \overline{\tau}_s'(s_0) = -\lambda_s \frac{\cos\overline{\psi}}{\overline{r}} (\overline{\tau}_s + \overline{\gamma}). \quad (19)$$

We also have to introduce a modified effective surface tension $\overline{\gamma} = \lambda_\varphi / \overline{\lambda}_\varphi$, because the real surface area exceeds the pseudosurface area, and we have to model this increase of E_γ by increasing γ instead. This new system of differential equations is closed by the relations

$$\lambda_s = \frac{\overline{\tau}_s \overline{\lambda}_\varphi + Y_{2D}}{Y_{2D} - \nu\gamma}, \quad \overline{\lambda}_\varphi = \frac{\overline{r}}{r_0}.$$

In order to calculate $\overline{\gamma}$, the circumferential stretch factor λ_φ of the *real, wrinkled* surface has to be calculated via the constitutive relations (13). To calculate wrinkled capsule shapes we start to solve the shape equations (17) as described before. As soon as the condition $\tau_\varphi + \gamma < 0$ is valid, we continue the calculations by solving the modified system (19). By following the solution of the modified system, we can calculate the length L_w of the wrinkled region

$$L_w = \int_{\tau_\varphi + \gamma < 0} ds. \quad (20)$$

At this point, it is also possible to calculate the wavelength of the wrinkles using the same methods as in Ref. [17]. Here we will mainly be interested in the extent L_w of the wrinkled region.

4. Ferrofluid droplet

The special case $Y_{2D} = 0$ describes a ferrofluid droplet without an elastic shell and has been treated in the literature before. The balance of forces on the surface is given by the Laplace-Young equation (12). Using the definitions of κ_s and κ_φ, this equation can be translated into

$$\frac{d\psi}{ds} = \frac{p}{\gamma} - \frac{\sin\psi}{r}.$$

In order to have a parametrization in the reference arc length s_0 and a fixed integration interval, we introduce a constant stretch factor λ_s, which is adjusted as a shooting parameter. The boundary and matching conditions are the same as in the case of the elastic shape equations. Together with the already known geometrical relations for r and z, we get a system of three shape equations for a droplet:

$$r'(s_0) = \lambda_s \cos\psi, \quad z'(s_0) = \lambda_s \sin\psi, \quad \psi'(s_0) = \lambda_s \left(\frac{p_0 + f_m}{\gamma} - \frac{\sin\psi}{r} \right). \quad (21)$$

This system is solved in the same way as the shape equations for elastic capsules in the previous sections. The basic shooting parameters are given by λ_s and p_0. Our solution scheme for the Laplace-Young equation is chosen such that it is completely analogous and comparable to the elastic shape equations. There are several other ways to solve this equation with a volume constraint, for example, by employing finite elements [65].

D. Iterative numerical solution of the coupled problem

The magnetostatic and the elastic problem are coupled: The capsule shape determines the boundary conditions for the magnetic field via the continuity conditions (5), while the normal magnetic force density $f_m(r,z)$ acting on the capsule surface [see Eq. (3)] enters the shape equations (17) via the pressure [see Eq. (16)]. To find a joint solution we use an iterative numerical solution scheme. We start with the reference shape and calculate the corresponding magnetic field $\mathbf{H}(r,z)$ for a given external field $\mathbf{H}_0$. Then we can calculate a deformed shape of the capsule using this magnetic field.

Now we recalculate the magnetic field and so on until the iteration converges. At this fixed point, the solution of the shape equations and the magnetic field are self-consistent. This iterative coupling of elastic shape equations to an external field calculated by a boundary element method is similar to the iterative scheme used in Ref. [11] to calculate the shape of sedimenting capsules in an external flow field. For the problem of ferrofluid droplets, an analogous iterative strategy has been introduced in Refs. [34,54,55,59].

The iteration can cause numerical problems in the solution of the the nonlinear elastic shape equations. If the capsule shape changes rapidly during the iteration, the shooting method used to solve the shape equations does not find a solution. This problem can be reduced by slowing down the iteration. To solve the elastic shape equations in the nth step, we use a convex linear combination of the updated magnetic field $\mathbf{H}_n'$ and the magnetic field $\mathbf{H}_{n-1}$ from the previous iteration step instead of $\mathbf{H}_n'$ itself [11,59]:

$$\mathbf{H}_n = \mathbf{H}_{n-1} + \alpha(\mathbf{H}_n' - \mathbf{H}_{n-1}). \tag{22}$$

The parameter α ranges between 0 and 1 and has to be lowered in situations of quickly changing shapes of the capsule. Finally, it is switched back to 1 to ensure real convergence. To track a solution as a function of the magnetic field strength, it is helpful to increase the external magnetic field $\mathbf{H}_0$ in small steps $\Delta\mathbf{H}_0$ and let the capsule's shape converge after each step. This slows down the calculation speed drastically but increases numerical stability and helps to track a specific branch of stable solutions (see Sec. IV C 4).

A problem with the iterative solution scheme can arise if the capsule shape becomes nearly conical with a very sharp tip of high curvature. Then the numerical error in the calculation of the magnetic field (see Sec. II B 2) makes it difficult or even prohibitive to reach a fixed point of the iterative scheme. Instead the iteration gives oscillations of the capsule shape around the required fixed point, which worsens the quality of the results. The iterative strategy used here directly converges to stationary shapes without simulation of the real dynamics.

An alternative to our iterative scheme is to directly simulate the dynamics for the fluid from the electromagnetic, elastic, and hydrodynamic forces. Then the fluid motion is simulated over time until it reaches a steady state. This method was used by Karyappa *et al.* for elastic capsules in electric fields [21]. For liquid droplets, there are comparable problems with sharp tips and numerical singularities, where the full dynamics could by solved to great accuracy, such as the emission of fluid jets at the tip of drops in electric fields [43], pinch-off dynamics [66], and coalescence phenomena [67]. The errors of the field calculation with finite elements at such sharp tips can also be reduced by using advanced mesh algorithms, such as the elliptic mesh generation [68].

E. Control parameters and nondimensionalization

In order to identify the relevant control parameters and reduce the parameter space, we introduce dimensionless quantities. We measure lengths in units of the radius R_0 of the spherical rest shape, energies in units of γR_0^2, i.e., tensions in units of the surface tension γ of the ferrofluid, and magnetic fields in units of the external field H_0. The problem is then governed by essentially three dimensionless control parameters.

The magnetic Bond number B_m,

$$B_m \equiv \frac{\mu_0 R_0 \chi H_0^2}{2\gamma}, \tag{23}$$

is the dimensionless strength of the magnetic force density. With this dimensionless number, the Laplace-Young equation (12) for a ferrofluid droplet can be written in dimensionless form

$$\tilde{\kappa}_s + \tilde{\kappa}_\varphi = \tilde{p}_0 + B_m\left(\tilde{H}^2 + \chi \tilde{H}_n^2\right),$$

with $\tilde{H} \equiv H/H_0$, $\tilde{\kappa} \equiv R_0\kappa$, and $\tilde{p} \equiv pR_0/\gamma$. The scaled droplet shape described by this Laplace-Young equation then only depends on the two dimensionless parameters B_m and χ.

The dimensionless Young modulus Y_{2D}/γ is the control parameter for elastic properties of the capsule shell. Another dimensionless control parameter for elastic properties is Poisson's ratio ν, which is set to $\nu = 1/2$ and thus fixed throughout this paper. The limit $Y_{2D}/\gamma = 0$ describes a droplet without an elastic shell while $Y_{2D}/\gamma \gg 1$ describes a system dominated by the shell elasticity.

The three dimensionless parameters B_m, Y_{2D}/γ, and the magnetic susceptibility χ of the ferrofluid uniquely determine the capsule shape (apart from its overall size R_0). In the following we consider Bond numbers B_m between 0 and 10^3 (see Sec. IV). For a typical ferrofluid-filled capsule with $\chi = 21$, $R_0 = 1$ mm [21,69], and $\gamma = 0.01$ N/m, these Bond numbers correspond to magnetic field strengths H between 0 and about 500 kA/m (or fields $B = \mu_0 H$ between 0 and 0.5 T). We consider dimensionless Young moduli Y_{2D}/γ from 10^{-2} (nearly no elasticity) to 100 (elastically dominated) and the purely elastic limit $Y_{2D}/\gamma = \infty$ (where the definition of B_m is not useful anymore). For the analogous problem of a dielectric droplet in an external electric field E_0 we can introduce a dielectric Bond number B_e by $B_e = \varepsilon_0 \varepsilon_{\text{out}} R_0 \chi_\varepsilon E_0^2/2\gamma$, where χ_ε is the analog of the magnetic susceptibility χ and has been defined in Eq. (8).

III. ANALYTICAL APPROACHES

In this section we introduce three approximative analytical approaches to the problem, which describe ferrofluid-filled elastic capsules in three different deformation regimes. The first approach is the analysis of the linear response of the capsule to small magnetic forces. The second approach applies to spheroidal shapes at moderate magnetic forces and is an approximative minimization of the total magnetic and elastic energy under the assumption of a spheroidal shape and uniform stretch factors. This extends the approximative energy minimization of Bacri and Salin [27] for ferrofluid droplets to capsules. Finally, we investigate conical capsule shapes as they can arise under strong magnetic forces. We investigate the existence of conical shapes and derive the governing equations in a slender-body approximation by extending the approach of Ref. [32] from conical droplets to conical capsules.

A. Linear shape response at small fields

In this section we derive the linear response of the spherical capsule shape to small magnetic forces. In particular, we derive the elongation a/b of the capsule, where a denotes the capsule's polar radius and b its equatorial radius (see Fig. 1). Details of the derivation are given in Appendix A; here we present the main results.

At small fields displacements change linearly in the magnetic force density f_m. Therefore, radial and tangential displacements $u_R(\theta)$ and $u_\theta(\theta)$ (using spherical coordinates with a polar angle θ and assuming axisymmetry) are of $O(H^2)$. In order to calculate the displacements we consider the force equilibria in normal direction, i.e., the Laplace-Young equation (14), and in tangential direction, i.e., Eq. (15). For a liquid ferrofluid droplet with an isotropic surface tension γ both force-equilibria give equivalent results. Expanding to linear order in the displacements around the spherical shape, we obtain two coupled differential equations for the functions u_R and u_θ.

These linearized force-equilibrium equations can be solved exactly. The solution takes the form

$$u_R = A + B\cos^2\theta, \quad u_\theta = C\sin\theta\cos\theta, \tag{24}$$

where A, B, and C are determined in Appendix A explicitly. We find $B = \mu_0(5+\nu)\chi^2 H^2 R_0^2/8[Y_{2D} + (5+\nu)\gamma]$ from the normal force equilibrium and $C = -2(1+\nu)B/(5+\nu)$ from the tangential force equilibrium and the pressure is adjusted such that $A = -B/3$ in order to fulfill the volume constraint.

The functional form $u_R = A + B\cos^2\theta$ of the normal displacement leads to a spheroidal shape in linear response. For a spheroid we can use the relation $H = 3H_0(3+\chi)$ and obtain $B = R_0 B_m 9(5+\nu)\chi/4(3+\chi)^2[Y_{2D}/\gamma + (5+\nu)]$. The linear response approach remains valid as long as $A, B, C \ll R_0$ or $B_m/[Y_{2D}/\gamma + (5+\nu)] \ll (3+\chi)^2/\chi \approx \chi$.

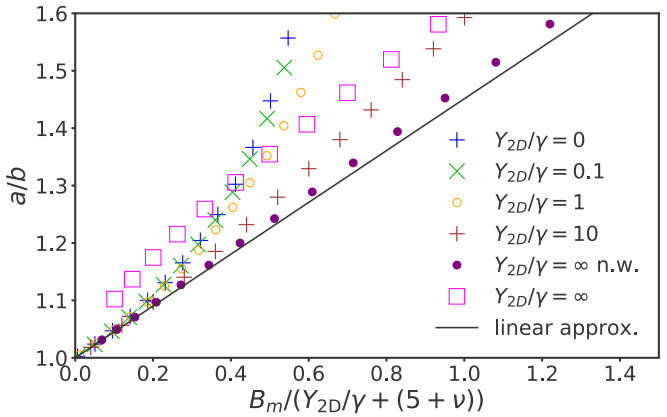

FIG. 4. Elongation a/b of a capsule filled with a ferrofluid with $\chi = 21$ as a function of $B_m/[Y_{2D}/\gamma + (5+\nu)]$ for different values of Y_{2D}/γ in the region of small deformations. The solid line describes the linear approximation from Eq. (25). The best agreement between the numerical data and the linear approximation is given for a purely elastic system without wrinkling effects (closed purple circles). Wrinkling effects lead to considerable deviations (squares).

From the displacement $u_R(\theta)$ we can calculate its elongation

$$\frac{a}{b} \approx 1 + \frac{u_R(0) - u_R(\pi/2)}{R_0} = 1 + \frac{B}{R_0}$$

in linear order in the displacement. For a ferrofluid droplet with surface tension γ and without any elastic tensions, i.e., $Y_{2D}/\gamma = 0$, we get, for the elongation a/b in linear order [see Eq. (A10)],

$$\frac{a}{b} = 1 + \frac{9\mu_0 R_0 \chi^2}{8\gamma(3+\chi)^2} H_0^2.$$

For the general case $Y_{2D}/\gamma > 0$, we find [see Eq. (A16)]

$$\frac{a}{b} = 1 + \frac{9\mu_0 R_0 \chi^2 (5+\nu)}{8[Y_{2D} + \gamma(5+\nu)](3+\chi)^2} H_0^2 = 1 + \frac{9}{4}\frac{\chi}{(3+\chi)^2}\frac{B_m}{Y_{2D}/\gamma(5+\nu)+1}, \tag{25}$$

which gives a precise prediction of the capsule's elongation for small fields, as a comparison with the numerical results in Fig. 4 shows. To leading order in B_m Eq. (25) agrees with the results from a similar small deformation approach in Ref. [21] for capsules filled with a dielectric liquid in electric fields.

B. Approximative energy minimization for spheroidal shapes

In this section we derive an analytical approximation for the elongation a/b of the capsule at moderate magnetic forces by minimizing an approximative total energy, which assumes a spheroidal shape for magnetic and elastic contributions. For ferrofluid droplets, the spheroidal approximation is based on the experimental observation that the droplet shape in uniform magnetic fields is very similar to a prolate spheroid [26,27,35] for sufficiently small magnetic Bond numbers before a transition into a conical shape can take place. Our numerical results show that this behavior remains qualitatively unchanged with an additional elastic shell (see Sec. IV A).

Therefore, we consider a capsule with prolate spheroidal shape. Analogously to Bacri and Salin [27], we use an energy argument by minimizing the total energy of the capsule at fixed volume $V = (4\pi/3)ab^2 = V_0$. The total energy consists of three different contributions. First is the surface energy E_γ, which is caused by the surface tension γ. It is proportional to the surface area A and

given by

$$E_\gamma = \gamma A = 2\pi ab\left[\frac{b}{a} + \frac{1}{\epsilon}\arcsin\epsilon\right]\gamma, \tag{26}$$

where $\epsilon \equiv \sqrt{1 - b^2/a^2}$ is the eccentricity.

The second energy contribution is the magnetic field energy E_{mag}. According to Ref. [70], E_{mag} can be written as

$$E_{\mathrm{mag}} = -\frac{V\mu_0}{2}\frac{\chi}{1+n\chi}H_0^2 \tag{27}$$

for $\mu_{\mathrm{out}} = 1$ and with the demagnetization factor $n = (b^2/2a^2\epsilon^3)\{-2\epsilon + \ln[(1+\epsilon)/(1-\epsilon)]\}$.

The third energy contribution is the elastic stretching energy E_{el}, which we construct by taking the energy density w_s from Sec. II C,

$$E_{\mathrm{el}} = \int w_s dA_0 = \int \frac{1}{2}\frac{Y_{2D}}{1-\nu^2}\left(e_s^2 + 2\nu e_s e_\varphi + e_\varphi^2\right)dA_0,$$

with $e_s = \lambda_s - 1$ and $e_\varphi = \lambda_\varphi - 1$, as defined in Sec. II C 1. At this point, the stretch factors λ_s and λ_φ are unknown and we need further approximations. An acceptable approximation for spheroidal shapes, which is checked below by comparison with the numerics (see Fig. 6), is constant stretch factors throughout the shell, i.e., $\lambda_s, \lambda_\varphi = \mathrm{const}$, which leads to

$$E_{\mathrm{el}} = \frac{1}{2}\frac{Y_{2D}}{1-\nu^2}\left(e_s^2 + 2\nu e_s e_\varphi + e_\varphi^2\right)A_0. \tag{28}$$

We approximate the circumferential stretch factor λ_φ by the stretching of a fiber at the capsule equator and set

$$\lambda_\varphi = \frac{b}{R_0}.$$

In meridional direction we approximate λ_s by taking the ratio of the perimeter P_{ellipse} of the corresponding ellipse, which generates the prolate spheroid by rotation, and the perimeter $P_{\mathrm{circle}} = 2\pi R_0$ of a great circle on the initial sphere. The perimeter of the ellipse is given by an elliptic integral. Therefore, we use Ramanujan's approximation [71], which leads us to

$$\lambda_s = \frac{P_{\mathrm{ellipse}}}{P_{\mathrm{circle}}} \approx \frac{a+b}{2R_0}\left(1 + \frac{3\eta^2}{10 + \sqrt{4-3\eta^2}}\right),$$

with $\eta \equiv (b-a)/(b+a)$.

As the last step, we have to minimize the total energy $E_{\mathrm{tot}} = E_\gamma + E_{\mathrm{mag}} + E_{\mathrm{el}}$ with respect to the elongation ratio a/b at fixed volume $V = (4\pi/3)ab^2 = V_0$ in order to get the equilibrium elongation as a function of the magnetic Bond number B_m for spheroidal shapes. Details of the calculation are presented in Appendix B. We obtain a closed but quite complicated analytical expression for the inverse relation $B_m = g(b/a)$, i.e., the magnetic Bond number B_m as a function of the inverse elongation $b/a < 1$ for spheroidal shapes in Eq. (B1). The function $g(k)$ in Eq. (B1) still depends on three dimensionless parameters: the susceptibility χ, the dimensionless Young modulus Y_{2D}/γ, and Poisson's ratio ν. This relation reduces to the results of Bacri and Salin [27] for ferrofluid droplets in the limit $Y_{2D} = 0$.

C. Conical membrane shapes with normal magnetic forces

For ferrofluid-filled droplets a shape transition into a stable conical shape with $\psi(0) > 0$ is possible above a critical susceptibility χ_c and at high magnetic fields [27,30,32,72]. We want to show that a conical shape with a strictly conical tip can also exist for an elastic capsule with spherical rest

shape and normal magnetic stretching forces if the constitutive relation is of the nonlinear form (13). Details of the argument are presented in Appendix C.

The existence of sharp cones in deformed membranes is an important issue in deformations of membranes with planar rest shape [73]. A membrane of thickness D prefers bending deformations (energy proportional to D^3) over stretching deformations (energy proportional to D). If external forcing or constraints are such that stretching can be avoided, the membrane responds by pure bending. Any deformation of such an unstretched membrane has to preserve the metric and thus the vanishing Gaussian curvature of a plane. This results in so-called developable cones, which have zero Gaussian curvature everywhere except at the tip of the cone. Cones only develop in response to external forces or constraints, typically under compressional constraints or forcing as in the crumpling of paper. Then unstretched membranes develop folds or wrinkles around the developable cones in order to accommodate the excess area that occurs under compression [73–75].

Our ferrofluid elastic membranes differ in several respects. The magnetic forces are always *stretching* forces and they are always *normal* to the surface such that the tangential force equilibrium (15) only involves internal stresses of the membrane. Under stretching forces the membrane cannot respond by pure bending and changes in the metric are unavoidable. However, the forcing depends on the magnetic field distribution [see Eq. (3)] and becomes concentrated in points of high fields, which are typically points of high curvature. This establishes a positive feedback between shape and magnetic field distribution that can stabilize conical tips. Moreover, we consider membranes with spherical rest shape and thus nonzero Gaussian curvature $K = 1/R_0^2$. This is another reason why deformation into a cone with $K = 0$ is impossible without stretching. Similar conditions (normal forces and spherical rest shape) are fulfilled for spherical shells under point forces, where conical solutions have also been obtained [13] and to which most of our results regarding the existence of conical shapes should also apply.

The tangential force equilibrium (15) has to be fulfilled in the vicinity of the conical tip and is independent of the stretching magnetic forces, which are always normal. In combination with the nonlinear constitutive relations (13) this requires that the stretching tensions remain finite and isotropic at the conical tip, i.e., $\tau_s(0) = \tau_\varphi(0) > 0$ at $s_0 = 0$. From the constitutive relations then also follows the isotropy of the stretches $\lambda_s(0) = \lambda_\varphi(0)$ at the tip. However, stretches are not necessarily finite at a conical tip.

For finite isotropic stretches $\lambda_s(0) = \lambda_\varphi(0) < \infty$ at the pole, l'Hôpital's rule applied at $s_0 = 0$ gives $\lambda_\varphi(0) = \lambda_s(0)\cos[\psi(0)]$ [see Eq. (C2)]. Then isotropy requires $\psi(0) = 0$ and it follows that a sharp conical tip with $\psi(0) > 0$ is impossible if stretches remain finite at the tip. Finite isotropic stretches at the pole thus always lead to flat tips with $\psi(0) = 0$ as for the spheroidal shapes.

For diverging and asymptotically isotropic stretches

$$\lambda_s(s_0) \approx \lambda_\varphi(s_0) \approx \text{const}\, s_0^{-\beta}, \tag{29}$$

with an exponent $\beta > 0$; however, l'Hôpital's rule does not apply at $s_0 = 0$. Then we find instead that isotropy of the diverging stretches requires a conical tip with the relation

$$\beta = \cos[\psi(0)] - 1 = \sin\alpha - 1 \tag{30}$$

between the exponent β and the half opening angle $\alpha = \pi/2 - \psi(0)$ of the conical tip [see Eq. (C4)]. This result can be obtained from a modified l'Hôpital's rule or directly from analyzing stretches for a deformation into a conical tip under the constraint of isotropy of the stretches at the tip [see Eq. (C12)]. For the nonlinear constitutive relation (13) diverging and isotropic stretches are still compatible with finite and isotropic tensions, which approach $\tau_s(0) = \tau_\varphi(0) = Y_{2D}/(1-\nu)$ [see Eq. (C5)] at the tip. Moreover, $\beta > -1$ according to (30) and therefore the divergence is such that the elastic energy [the energy density (10) integrated over the tip area] remains finite.

Any numerical approaches to capsule shell mechanics and the calculation of the magnetic fields rely on discretization. In the numerical solution of axisymmetric shape equations, the arc length s_0 is discretized. After discretization in the numerics, stretches necessarily remain finite at potential

conical tips at the apices. Then our results for finite stretches apply and we have to choose a boundary condition $\psi(0) = 0$. Also, for the calculation of the magnetic fields, we discretize the boundary of the capsule [see Eq. (7)]. Therefore, also magnetic fields remain finite at conical tips. Then also the normal magnetic forces remain finite and can only support finite curvatures at the tip of the conical shape. This leads to a rounding of conical tips and thus also requires $\psi(0) = 0$. This implies that, in the numerical calculations, all shapes of ferrofluid capsules will have rounded tips with $\psi(0) = 0$; the rounding of a conical tip for these numerical reasons will happen on the scale of the discretization of the problem. A boundary condition $\psi(0)$ for the numerical solution of the shape equations [see Eq. (18)] has also been used in Refs. [34,54,55,59] for ferrofluid droplet shapes.

D. Slender-body approximation for conical capsules

For ferrofluid droplets, the conical shape could be investigated analytically using a slender-body approximation [32], which we want to adapt for conical shapes of the ferrofluid-filled capsule. We have shown that conical shapes can also exist for ferrofluid-filled capsules, but they involve diverging isotropic stretches at the conical tip. Tensions are isotropic, remain finite at the conical tip, and approach the limiting values $\tau_s(0) = \tau_\varphi(0) = Y_{2D}/(1-\nu)$ [see Eq. (C5)].

The capsule shape is described by a function $r(z)$ in cylindrical coordinates. In a slender-body approximation, we assume $\partial_z r \ll 1$; for a conical tip with half opening angle $\alpha = \pi/2 - \psi(0)$, we have $\partial_z r \approx \tan\alpha$ in the vicinity of the tip. Then we can neglect small radial field components and approximate the magnetic field as parallel to the z axis, $\mathbf{H} = H(z)\mathbf{e}_z$. The field $H(z)$ is determined by

$$H_0 = H(z) - \frac{\ln A}{2}\chi\,\partial_z^2[r^2(z)H(z)], \tag{31}$$

where A is the aspect ratio of the slender shape, which can be expressed in terms of the half opening angle, $A = 1/\tan\alpha$, for a conical shape [32]. This relation is unchanged as compared to fluid droplets as it is a result of the slender shape and magnetic boundary conditions only and independent of the surface elasticity underlying the shape.

In the slender-body approximation we also assume $\partial_z^2 r \ll 1/r$ such that the meridional curvature is small $\kappa_s \ll \kappa_\varphi \approx 1/r(z)$. Then the Laplace-Young equation describing normal force equilibrium becomes

$$\frac{1}{r(z)}\{\tau_\varphi[r(z)] + \gamma\} = p_0 + f_m. \tag{32}$$

This relation differs from the corresponding relation for fluid droplets by the appearance of the additional elastic tension $\tau_\varphi = \tau_\varphi(r)$. As shown in Appendix C 3, tangential force equilibrium is fulfilled in the vicinity of the conical tip if stretches are diverging, and the resulting circumferential tension is

$$\tau_\varphi(r) = \frac{Y_{2D}}{1-\nu}[1 - 2R_0\sin\alpha(a\tan\alpha)^{-1/\sin\alpha} r^{1/\sin\alpha - 1}] \tag{33}$$

[see Eq. (C14)] in the vicinity of the conical tip. Note that a still denotes the polar radius. In Appendix C 2 we also outline how the tension $\tau_\varphi(r)$ could be calculated for a general shape $r(z)$, in principle.

The Laplace-Young equation (32) with an elastic tension (33) and the slender-body field equation (31) provide two coupled equations for $r(z)$ and $H(z)$. The pressure p_0 has to be chosen such that the resulting shape $r(z)$ fulfills the volume constraint

$$V_0 = \pi\int_{-a}^{a} r^2(z)dz. \tag{34}$$

The three equations (31), (32), and (34) governing slender (and, in particular, conical) shapes of a ferrofluid-filled capsule only differ in the appearance of the additional elastic tension $\tau_\varphi = \tau_\varphi(r)$

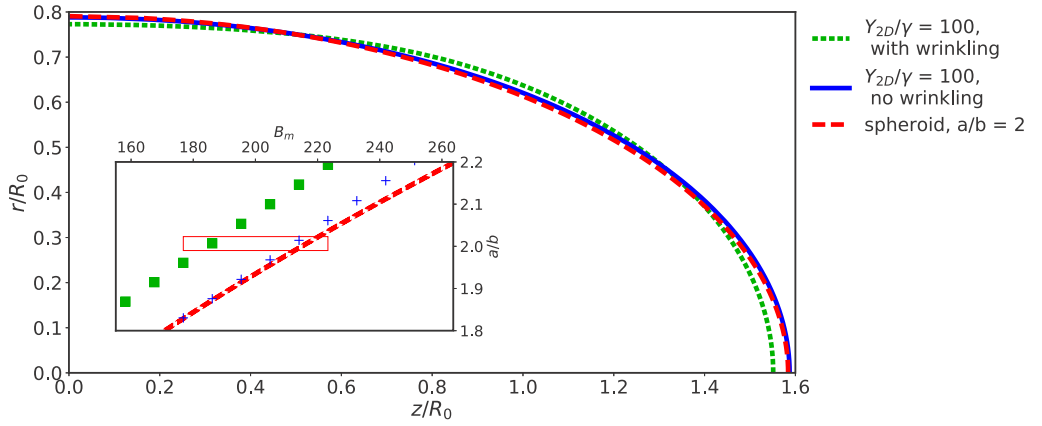

FIG. 5. Comparison of numerically calculated $r(z)$ contour of a capsule with $Y_{2D}/\gamma = 100$ and $\chi = 21$, for a value B_m chosen such that the elongation is $a/b = 2$ (the inset shows the location of the pictured shapes in the B_m-a/b plane) with a spheroid. The shape calculated without wrinkling (blue solid line) shows very good agreement with a spheroid of the same volume and elongation (red dashed line). Taking wrinkling into account leads to visible deviations (green dotted line).

from the corresponding equations for ferrofluid droplets from Ref. [32]. They can be also be solved analogously as for ferrofluid droplets, in principle.

IV. RESULTS

A. Spheroidal capsule shapes

While the capsule is spherical at $B_m = 0$, it becomes elongated for increasing magnetic field or Bond number B_m similarly to a ferrofluid droplet. We can quantify the elongation by the ratio of capsule length a in the z direction and capsule diameter b at the equator, a/b. At small or moderate magnetic fields ferrofluid capsules assume a prolate spheroidal shape to a very good approximation; one example is shown in Fig. 2(b).

For small fields we calculated the linear response of the capsule exactly in Sec. III A and Appendix A and found displacements (24), which describe a prolate spheroid with an elongation $a/b > 1$ given by Eq. (25). This analytical result is in excellent agreement with numerical results for small fields (see Fig. 4). The linear response regime is valid as long as $a/b - 1 \ll 1$ or $B_m \ll [Y_{2D}/\gamma(5+\nu)+1](3+\chi)^2/\chi$ according to Eq. (25).

Small magnetic fields are easily accessible and for many ferrofluids, susceptibilities are rather small (for example, $\chi \simeq 0.36$ in Ref. [36]). Therefore, spheroidal shapes in the linear response regime are experimentally easily accessible. Then the linear response relation (25) can be used as experimental method to deduce unknown capsule material properties, for example, Young's modulus Y_{2D} if the magnetic properties of the ferrofluid are known.

At moderate magnetic fields, the capsule shape remains very similar to a prolate spheroid for all elongations $a/b \lesssim 3$, which was one basic assumption of the approximative energy minimization in Sec. III B. Figure 5 demonstrates this for shapes with $a/b = 2$. The spheroidal approximation works better for systems dominated by the surface tension, i.e., for small ratios Y_{2D}/γ. For fixed Bond number B_m and susceptibility χ the elongation decreases with increasing Y_{2D}/γ because of the additional stretching energy of the shell as compared to a droplet, so a ferrofluid droplet ($Y_{2D}/\gamma = 0$) always shows the highest elongation. For small fields, this trend can be quantified with the linear response relation (25). For smaller elongations, the spheroidal approximation tends to work better.

The other assumption in the approximative energy minimization in Sec. III B was constant stretch factors throughout the shell, i.e., $\lambda_s, \lambda_\varphi = \text{const}$ (and thus constant elastic tensions τ_φ and τ_s).

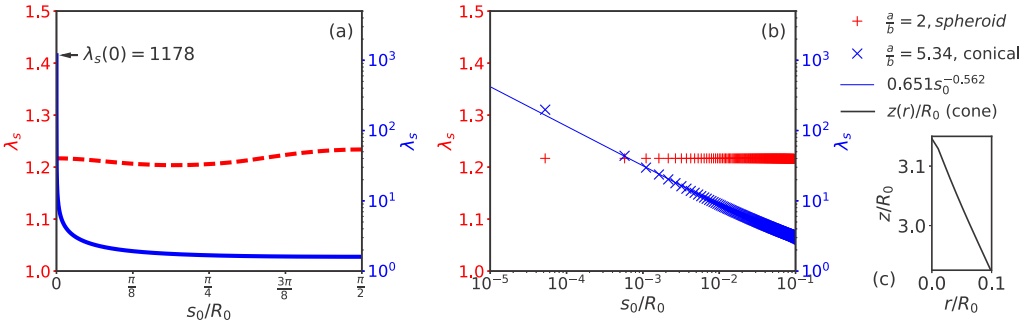

FIG. 6. (a) Stretch factors in the meridional direction $\lambda_s(s_0)$ following the whole contour line from the south pole ($s_0 = 0$) to the equator ($s_0/R_0 = \pi/2$) for $Y_{2D}/\gamma = 100$ and $\chi = 21$. The left scale (red dashed line) gives almost constant stretch factors for a spheroidal shape with $a/b = 2$. The right scale (blue solid line) gives diverging stretch factors for a conical shape with $a/b = 5.34$. (b) Logarithmic plot of $\lambda_s(s_0)$ near the tip for $s_0/R_0 < 10^{-1}$. The function $\lambda_s(s_0) = \text{const}\, s_0^{-\beta}$ [see Eq. (29)] was fitted to the data of the conical shape, which gave $\beta = 0.562$, corresponding to an angle $\alpha = 25.98^\circ$ in Eq. (30). (c) Zoom in to the tip of the contour line $z(r)$ for the conical shape; the half opening angle is $\alpha \approx 25^\circ$.

Also this approximation works very well for spheroidal shapes with elongations $a/b \lesssim 3$, as the numerical results in Fig. 6 for $a/b = 2$ (left scale, red line) show. As a result, the approximative energy minimization in Sec. III B gives very good results for moderate magnetic fields, i.e., for all elongations $a/b \lesssim 3$, where we always find prolate spheroidal shapes, as the comparison with numerical results in Fig. 7 shows.

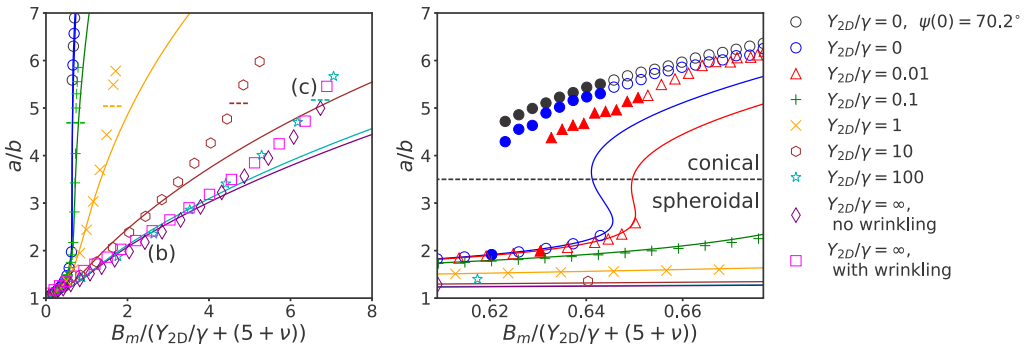

FIG. 7. Elongation a/b of a capsule filled with a ferrofluid with $\chi = 21$ as a function of magnetic Bond number B_m for different values of the dimensionless elastic parameter Y_{2D}/γ. The magnetic Bond number is rescaled by $Y_{2D}/\gamma + (5 + \nu)$, which is motivated by the small field behavior [see Eq. (25)]. The solid lines describe the theoretical results from approximative energy minimization (see Sec. III B). Open (closed) symbols denote numerical data for increasing (decreasing) B_m. The agreement is good for small elongations; the approximation fails for higher elongations, especially at the shape transition (close-up in the right diagram), where a/b jumps for small changes of B_m. Hysteresis effects are clearly visible in that area. There are two sets of numerical data for $Y_{2D}/\gamma = \infty$: Square data points are based on the modified shape equations that take wrinkling into account, while diamonds are calculated without wrinkling. There are also two sets of data without elasticity: The upper data points (black) describe a droplet with a real conical tip with a cone angle of $\psi(0) = 70.2^\circ$, as it was given in Ref. [32]; for the lower points (blue) we used the boundary condition $\psi(0) = 0$. Dashed lines indicate the position of shape transitions. Above these lines, shapes are conical, while they are spheroidal below. The markers (b) and (c) correspond to the shapes in Fig. 2.

B. Conical capsule shapes and capsule rupture

For large magnetic fields or Bond numbers B_m and at sufficiently high susceptibilities χ, ferrofluid capsules can also assume conical shapes, such as the shape in Fig. 2(c), which have also been found for ferrofluid droplets [30,32]. We investigated the possibility of conical shapes for elastic capsules with normal magnetic forces above in Sec. III C and found that stretch factors have to diverge at the conical tips, $\lambda_s(s_0) \approx \lambda_\varphi(s_0) \approx \text{const}\, s_0^{-\beta}$ [see Eq. (29)], with an exponent $\beta = \sin\alpha - 1$, which is determined by the half opening angle $\alpha = \pi/2 - \psi(0)$ of the conical tip [see Eqs. (30) and (C4)]. This behavior is confirmed by our numerical results in Fig. 6 (left scale, blue line). The stretch factors diverge but are asymptotically isotropic at the tips. The nonlinear constitutive relations (13) then result in finite and isotropic tensions $\tau_s(0) = \tau_\varphi(0) = Y_{2D}/(1-\nu)$ [see Eq. (C5)].

Diverging stretch factors cannot be realized in an actual material without rupture. Typical alginate capsule materials can only resist stretch factors of $\lambda \simeq 1.2$ before rupture; highly stretchable hydrogels can resist stretch factors up to $\lambda \sim 20$ [76]. Therefore, a real capsule should rupture at the poles at the transition into a conical shape and we conclude that investigations of conical shapes are primarily of theoretical interest. Such rupture events have actually been observed in Ref. [21] for capsules filled with a dielectric liquid in external electric fields. We expect that the nonlinear Hookean material law will become invalid at such high stretch factors prior to rupture. Then constitutive relations which are more realistic for high strains should be used. Nevertheless, the appearance of large stress factors is a robust feature of the conical shape independently of the material law.

Conical shapes cannot be described quantitatively by the approximative energy minimization from Sec. III B as spheroidal shapes with a large elongation a/b, which is clearly shown by the deviations between numerical results (data points) and the approximative energy minimization from Sec. III B (solid lines) for the conical shapes in Fig. 7. For ferrofluid droplets, conical shapes can be described by a slender-body theory [32], which we generalized in Sec. III D to ferrofluid-filled capsules. The three governing equations (31), (32), and (34) from Sec. III D can be used to describe conical capsule shapes quantitatively.

As pointed out above, the tensions remain finite and isotropic at the conical tip, i.e., $\tau_s(r) \approx \tau_\varphi(r) \approx Y_{2D}/(1-\nu)$ for small r [see Eq. (C5)]. Then the slender-body equation (32) from normal force balance actually becomes identical to the corresponding equation for a droplet from Ref. [32], however, with an effectively increased surface tensions $\gamma_{\text{eff}} = \gamma + \tau_\varphi(0)$. Also the other two equations (31) and (34) are identical such that we obtain very similar slender conical shapes for capsules and droplets, which can be mapped onto each other by a simple shift of the surface tension.

The mechanism underlying the stabilization of the conical shape is analogous to ferrofluid droplets because tensions remain finite and isotropic at the conical tip. A sharp conical tip with curvatures $\kappa_\varphi \propto 1/r$ gives rise to diverging magnetic fields $H \propto r^{-1/2}$ and normal magnetic forces

$$f_m \propto H^2 \propto r^{-1}, \tag{35}$$

both for ferrofluid droplets and capsules. These strong magnetic stretching forces stabilize the conical tip against high elastic restoring forces. The normal component of the elastic force is mainly due to the finite circumferential tension $\gamma + \tau_\varphi(0)$ acting along the high circumferential curvature $\kappa_\varphi \propto 1/r$ at the conical tip, resulting in an elastic force $f_{\text{el}} \propto [\gamma + \tau_\varphi(0)]\kappa_\varphi \propto r^{-1}$ with the same divergence. Magnetic and elastic normal forces balance in the Laplace-Young equation (32) in the slender-body approximation. The magnetic field exponent $H \propto r^{-1/2}$ is *identical* for capsules and droplets, as long as the elastic tensions at the conical tip are finite. This exponent determines the critical susceptibility χ_c above which a shape transition into conical shapes is possible and therefore we also find the identical χ_c for capsules and droplets as discussed in the following section.

C. Spheroidal-conical shape transition of capsules

Upon increasing the magnetic field or the magnetic Bond number B_m at fixed capsule elasticity $Y_{2D}/\gamma > 0$ and for a sufficiently large and fixed ferrofluid susceptibility χ, we find a discontinuous

shape transition from spheroidal to conical capsule shapes, similar to what has been found for ferrofluid droplets ($Y_{2D}/\gamma = 0$) [27,30,32]. One of our main results is the diagram of capsule elongation a/b as a function of Bond number B_m in Fig. 7 for different values of elasticity parameters Y_{2D}/γ and for $\chi = 21$, where a lower spheroidal branch and an upper conical branch and a discontinuous transition between both branches can be identified. In the following sections we will discuss different aspects of this shape transition in more detail.

1. Critical susceptibility χ_c

For ferrofluid droplets, a discontinuous shape transition was observed in experiments [27,77] and numerical simulations [34,35] only for susceptibilities $\chi > \chi_c$, i.e., above a critical susceptibility χ_c. In Ref. [30] a value $\chi_c = \mu_c/\mu_{\text{out}} - 1 \simeq 16.59$ was found below which no conical shape can exist; the slender-shape approximation for droplets from Ref. [32], which we generalized to elastic capsules in Sec. III D, gives $\chi_c = 16e/3 \simeq 14.5$. The approximative energy minimization of Bacri and Salin [27], which we generalized to elastic capsules in Sec. III B, gives $\chi_c \simeq 19.8$ for ferrofluid droplets. Numerically, a range of $\chi_c \simeq 19$ to $\chi_c \simeq 19.5$ is observed [72]. The question arises whether a critical susceptibility χ_c can also be found for the existence of a discontinuous spheroidal-conical transition for ferrofluid-filled elastic capsules.

For given χ and half opening angle α of the conical shape electromagnetic boundary conditions determine the divergence $H \propto r^{\mu-1}$ of the field via the equation [30,31]

$$P_\mu(\cos\alpha)P'_\mu(-\cos\alpha) + (\chi+1)P_\mu(-\cos\alpha)P'_\mu(\cos\alpha) = 0. \tag{36}$$

Because of the finite elastic tension $\tau_\varphi(0)$ at the conical tip, the magnetic field at the tip of a conical capsule diverges with the same $\mu = 1/2$ [see Eq. (35)] as for a conical droplet. Therefore, we find the same critical susceptibility $\chi_c \simeq 16.59$, above which a conical solution can exist, for both capsules and droplets.

In the slender-body approach, Eq. (31) determines χ_c and applies unchanged to both slender conical droplets and ferrofluid-filled capsules. Also the magnetic field divergence $H \propto r^{-1/2}$ is identical in both cases, so the analysis of Eq. (31) predicts the same critical value $\chi_c = 16e/3 \simeq 14.5$ for ferrofluid-filled capsules as for ferrofluid droplets.

In particular, both the analysis of Eq. (36) and the slender-body approach predict that the value for χ_c to be *independent* of the Young modulus Y_{2D} of the capsule. This result is corroborated by our numerics for $\chi = 21$, where we *always* observe a spheroidal-conical shape transition, even for $Y_{2D}/\gamma \to \infty$ [see Eq. (7)].

This result is in contrast, however, to what we find using the approximative energy minimization for spheroidal shapes from Sec. III B. Analyzing Eq. (B1), $B_m = g(k) = g(b/a)$, for the saddle points of the function $g(k)$ gives the critical value of the susceptibility χ_c [the two equations $g'(k) = 0$ and $g''(k) = 0$ determine two critical parameter values $k = k_c$ and $\chi = \chi_c$]. Using this approach, we find a χ_c, which is strongly increasing with the Young modulus Y_{2D}/γ, such that we find $\chi_c > 21$ already for $Y_{2D}/\gamma > 0.015$, which clearly disagrees with all our numerical and analytical results. The reason for this disagreement is the failure of the approximative energy minimization to correctly describe conical shapes as discussed in Sec. IV B.

It is interesting to consider the robustness of our result of a Y_{2D}-independent χ_c that is identical to the χ_c for ferrofluid droplets with respect to the constitutive relation. We used the nonlinear Hookean constitutive relation (13), which can only support *finite* tensions at a conical tip, even for diverging stretches (see Sec. III C). A simple linear Hookean constitutive relation [missing the $1/\lambda$ factors in Eq. (13)] behaves differently and exhibits diverging tensions $\tau_\varphi \sim r^{-\sigma}$ with $\sigma > 0$ at a conical tip. Then tangential force equilibrium (C1) also requires $\tau_s \sim \tau_\varphi \sim r^{-\sigma}$ but with an anisotropy $\tau_\varphi/\tau_s = 1 - \sigma$. With the linear constitutive relation this in turn leads to stretches $\lambda_s \sim \lambda_\varphi \sim r^{-\sigma}$ with an anisotropy $\lambda_\varphi/\lambda_s = (1-\nu-\sigma)/(1-\nu+\nu\sigma) \equiv \delta$ or $\delta(\sigma) = (1-2\sigma)/(1+\sigma)$ for a Poisson ratio $\nu = 1/2$. Requiring this anisotropy in Eq. (C10) at a conical tip with half opening angle α leads to a modified differential equation (C11) and a divergence $\lambda_s \sim \lambda_\varphi \sim r^{1-1/\delta(\sigma)\sin\alpha}$. Consistency with

$\lambda_s \sim \lambda_\varphi \sim r^{-\sigma}$ then requires

$$\sigma = \frac{1}{\delta(\sigma)\sin\alpha} - 1 = \frac{1+\sigma}{1-2\sigma}\frac{1}{\sin\alpha} - 1,$$

which determines the divergence $\sigma = \sigma(\alpha)$ of tensions $\tau_s \sim \tau_\varphi \sim r^{-\sigma}$ as a function of the opening angle α. At the conical tip we have now curvatures $\kappa_\varphi \propto 1/r$ in combination with circumferential tensions $\tau_\varphi \sim r^{-\sigma}$ such that normal force balance also requires magnetic forces $f_m \propto H^2 \propto r^{-1-\sigma}$ [cf. Eq. (35)]. Thus, we have to use $\mu = 1 - \sigma(\alpha)$ instead of $\mu = 1/2$ in $H \propto r^{\mu-1}$ in Eq. (36) and obtain a modified equation for the cone angle α as a function of the parameter χ. This equation has a solution only above $\chi_c \simeq 40.5$ and thus the critical value χ_c is strongly increased for a strictly linear Hookean constitutive relation. Our numerical results corroborate this result as we find only spheroidal capsule shapes for a strictly linear constitutive relation at a susceptibility $\chi = 21$. This shows that the value of χ_c is very sensitive to changes in the constitutive relation and a measurement of χ_c allows us to draw conclusions about the constitutive relation of the capsule material.

2. Critical Bond numbers

Our numerical solutions of the shape equations show that the discontinuous spheroidal-conical shape transition that exists for ferrofluid droplets [27,30,32] persists for ferrofluid-filled elastic capsules and shows qualitatively similar features. Both for droplets and for capsules, the driving force of the shape transition is the lowering of the magnetic field energy in the conical shape. Above an upper critical Bond number $B_{m,c2}$ the spheroidal shape becomes unstable and the droplet or capsule deforms into a much more elongated, conical shape. This shape transition is discontinuous, i.e., the deformation into the conical shape is associated with a jump in a/b. The discontinuous transition between spheroidal to conical shapes also exhibits hysteresis: Lowering the Bond number starting from values $B_m > B_{m,c2}$, the conical shape becomes unstable at a lower critical Bond number $B_{m,c1}$ with $B_{m,c1} < B_{m,c2}$. The discontinuous spheroidal-conical transition only exists above the critical susceptibility χ_c. In other words, both droplets and capsules exhibit a line of discontinuous shape transitions in the χ-B_m plane for $\chi > \chi_c$, which terminates at a critical point located at $\chi = \chi_c$. The lines $B_{m,c1}(\chi)$ and $B_{m,c2}(\chi)$ are the limits of stability (spinodals) of this shape transition and meet in the critical point.

Figure 7 shows the capsule elongation with respect to B_m for different values of the dimensionless elastic parameter Y_{2D}/γ of the capsule. We choose $\chi = 21$, which is only slightly above χ_c. This ensures that we have a shape transition for a ferrofluid droplet (corresponding to the limit $Y_{2D}/\gamma = 0$), on the one hand, and relatively small and thus numerically more stable elongations in the conical shape, on the other hand. Figure 7 clearly shows a discontinuous jump in elongation and hysteresis effects also for capsules with $Y_{2D}/\gamma > 0$.

3. Stretch factors as an order parameter

The discontinuous jump in the elongation ratio a/b at the spheroidal-conical transition is difficult to localize for larger values of Y_{2D}/γ, as Fig. 7 shows. More suitable order parameters for the spheroidal-conical transition are the stretch factors λ_s and λ_φ. Because the stretch factors diverge at the tips of the conical shape (the divergence is only limited by numerical discretization effects), whereas they stay finite at the poles of spheroidal shape (see Fig. 6 and our above discussion), we can directly employ the stretch factor $\lambda_s(s_0 = 0)$ at one of the poles as a convenient order parameter.

For $\chi = 21$ and $Y_{2D}/\gamma = 100$, the shape transition occurs where a/b has a rather small jump from about 5.2 to 5.35 for increasing Bond number B_m, whereas the stretch factor $\lambda_s(s_0 = 0)$ exhibits a much bigger jump by a factor of more than 10, as demonstrated in Fig. 8. Also the shape hysteresis at the spheroidal-conical shape transition can be clearly seen for the order parameter $\lambda_s(s_0 = 0)$.

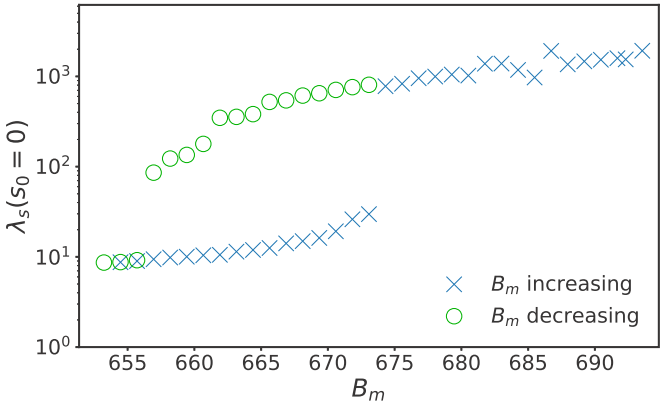

FIG. 8. Meridional stretch factor λ_s at the capsule pole $s_0 = 0$ as a function of Bond number B_m for $Y_{2D}/\gamma = 100$ and $\chi = 21$. The stretch factor clearly exhibits a jump at the location of the discontinuous shape transition and hysteretic behavior.

Using this order parameter, we can detect the spheroidal-conical shape transition of ferrofluid-filled capsules by the criterion

$$\lim_{\Delta B_m \to 0} |\lambda_s(s_0 = 0, B_m) - \lambda_s(s_0 = 0, B_m + \Delta B_m)| > 0, \tag{37}$$

where we use values $\Delta B_m = 0.005$ for $Y_{2D}/\gamma < 1$ up to values $\Delta B_m = 0.5$ for $Y_{2D}/\gamma = 100$ in practice [$B_{m,c1}$ and $B_{m,c2}$ grow approximately linearly with Y_{2D}/γ (see Fig. 9 below) such that larger values ΔB_m can be used for larger Y_{2D}/γ; smaller values of ΔB_m give more precise results]. For ferrofluid droplets, i.e., in the limit $Y_{2D}/\gamma \approx 0$, we still have to use jumps in the elongation a/b for small changes ΔB_m in the magnetic Bond number to detect the spheroidal-conical shape transition.

We note that the discretization problem at the sharp conical tip mentioned above causes high relative errors in the numerical values of stretch factors in the tip area. Therefore, our numerical results for the diverging stretch factors at the tips of conical capsule shapes cannot be numerically exact. The detection of a divergence in λ_s at the poles, which we use to detect the transition into a conical shape, is, however, still possible even in the presence of numerical errors.

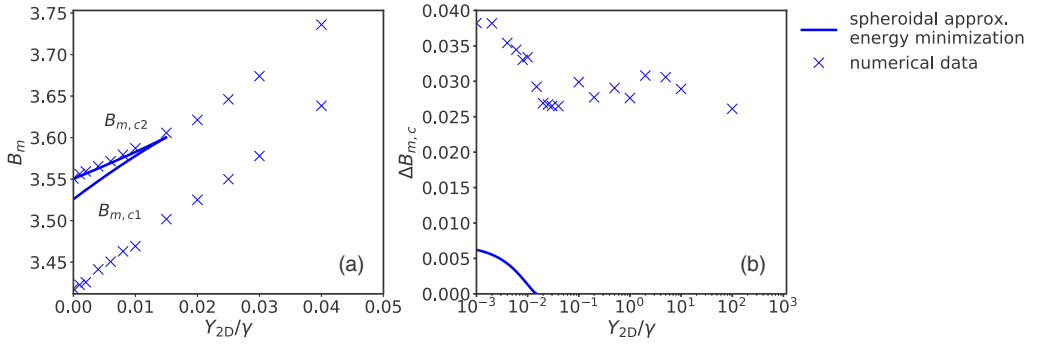

FIG. 9. (a) Critical Bond numbers $B_{m,c1}$ (lower data points) and $B_{m,c2}$ (upper data points) for varying Y_{2D}/γ with $\chi = 21$. The solid lines describe the prediction by the approximative energy minimization for spheroidal shapes. Both critical Bond numbers increase for increasing Y_{2D}/γ. In the region $B_{m,c1} < B_m < B_{m,c2}$ there are hysteresis effects in the spheroidal-conical shape transition. (b) Relative size $\Delta B_{m,c}$ of the hysteresis area for a wider range of Y_{2D}/γ.

4. Shape hysteresis

In order to track the range of elastic control parameters Y_{2D}/γ, where a discontinuous shape transition with hysteresis can be observed (for fixed $\chi = 21$), we use the stretch factor $\lambda_s(s_0 = 0)$ as the order parameter and the criterion (37) to determine $B_{m,c1}$ and $B_{m,c2}$. We determine $B_{m,c2}$ by increasing the Bond number in small steps $\Delta B_m > 0$ to locate the jump in the stretch factor $\lambda_s(s_0 = 0)$ at the pole, when the spheroidal shape becomes unstable. Analogously, we determine $B_{m,c1}$ by decreasing the Bond number in small steps $\Delta B_m < 0$ to locate the jump in $\lambda_s(s_0 = 0)$, when the conical shape becomes unstable (see Fig. 8).

Repeating this procedure for increasing values of the elastic control parameter Y_{2D}/γ, we obtain the location and size of the hysteresis loop $B_{m,c1} < B_m < B_{m,c2}$ for a fixed susceptibility as a function of Y_{2D}/γ (see Fig. 9). We see that $B_{m,c1}$ and $B_{m,c2}$ increase (approximately linear) for increasing Y_{2D}/γ because of the increasing elastic energy needed for the same deformation. Note that the absolute numerical values of $B_{m,c1}$ and $B_{m,c2}$ cannot be considered exact as they are depending on the discretization of the magnetic field calculation (see also Appendix D).

The approximative energy minimization for spheroidal shapes from Sec. III B can be used to calculate approximative values for $B_{m,c1}$ and $B_{m,c2}$ from Eq. (B1), $B_m = g(k) = g(b/a)$ [the two equations $g'(k) = 0$ and $B_m = g(k)$ determine the critical Bond numbers $B_m = B_{m,c1/2}$ and a corresponding critical inverse aspect ratio $k = k_c$]. We find that the hysteresis loop closes already for $Y_{2D}/\gamma > 0.015$ for $\chi = 21$ (see Fig. 9), which is equivalent to our above finding (see Sec. IV C 1) that $\chi_c > 21$ for $Y_{2D}/\gamma > 0.015$ in the approximative energy minimization. Comparison with our numerical results in Fig. 9 shows that the approximative energy minimization gives quite accurate results for the upper critical Bond number $B_{m,c2}$, i.e., the stability limit of the spheroidal shape. It fails completely to predict the lower critical Bond number $B_{m,c1}$, i.e., the stability limit of the conical shape, because it is not able to describe conical shapes quantitatively (see Sec. IV B).

The numerical calculation shows hysteresis behavior for *all* values of Y_{2D}/γ (see Fig. 9). Only the relative size of the hysteresis loop, $\Delta B_{m,c} \equiv 2(B_{m,c2} - B_{m,c1})/(B_{m,c2} + B_{m,c1})$, decreases slightly for increasing Y_{2D}/γ in the numerical results.

D. Wrinkling

1. Wrinkled shapes

As opposed to liquid droplets, elastic capsules can develop wrinkles if a part of the shell is under compressive stress [14–17]. Wrinkles have also been considered for the equivalent problem of capsules filled with a dielectric liquid in an external electric field in Ref. [21].

As it was stated in Sec. II C 3, wrinkles appear if the total hoop stress becomes compressive, $\tau_\varphi + \gamma < 0$. Then we have to use modified shape equations (19) in the numerical calculation of the shape.

As can be seen in Fig. 7, taking wrinkling into account has a visible effect on the capsule's elongation for higher values of Y_{2D}/γ. If wrinkling is taken into account capsules elongate because wrinkling reduces the compressional stretch energy, which is stored near the equator. This elastic energy gain can be used for a further elongation of the capsule at the same field strength to lower the magnetic energy. This also results in stronger deviation from the spheroidal shape. To visualize this effect, Fig. 5 shows the projection of the contour line of the upper right quadrant of capsules with and without wrinkling using the same elongation $a/b = 2$. While the shape is indistinguishable from a spheroid without wrinkling, the wrinkled shape deviates from a spheroid.

Also in the presence of wrinkling, the discontinuous spheroidal-conical shape transition where the elongation increases persists. In the following, we will focus on the effect of wrinkles on the spheroidal branch of shapes.

2. Extent of wrinkled region

In order to characterize the wrinkling tendency of spheroidal capsules we calculate the extent of the wrinkled region L_w [cf. Eq. (20) and Fig. 3], which can easily be measured in experiments. First

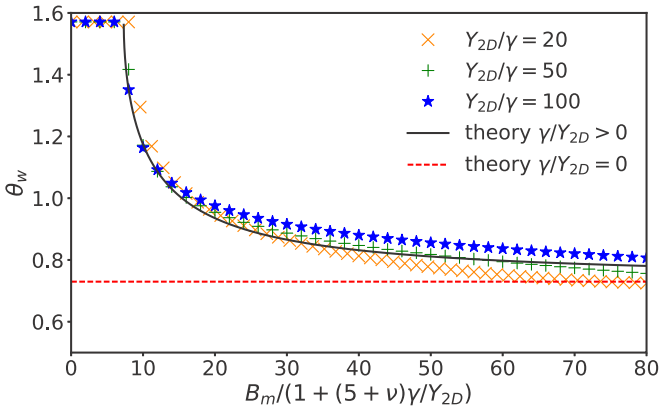

FIG. 10. Extent of the wrinkled region represented by the polar angle θ_w as a function of $B_m/[1+(5+\nu)\gamma/Y_{2D}]$. The lines are the linear response result (38), crosses and stars are numerical data points for different values of $Y_{2D}\gamma$, which all collapse to the linear response result. The red (dashed) line gives the asymptotic result $\cos^2\theta_w = 5/9$ for large values of $B_m/[1+(5+\nu)\gamma/Y_{2D}]$ and for purely elastic capsules ($\gamma/Y_{2D} = 0$).

we use the wrinkle criterion $\tau_\varphi + \gamma < 0$ to calculate the extent of the wrinkled region in the linear response regime for small magnetic fields as outlined in Sec. III A and Appendix A. In the linear response regime, we calculate the deviation from a sphere with radius R_0 to leading order. We can characterize the size of the wrinkled region in terms of the polar angle θ as $\theta_w < \theta < \pi - \theta_w$ where θ_w is the smallest polar wrinkle where wrinkles appear, $\tau_\varphi(\theta_w) + \gamma = 0$. This angle is related to the length L_w of the wrinkled region by $L_w = R_0(\pi - 2\theta_w)$: An angle of $\theta_w = \pi/2$ implies the absence of wrinkles, while $\theta_w = 0$ means that the wrinkles extend from pole to pole. Using Eq. (A17) for τ_φ, we find

$$\cos^2\theta_w = \frac{5}{9} - \frac{\gamma R_0}{Y_{2D}B}\frac{5+\nu}{3} = \frac{5}{9} - \frac{4(3+\chi)^2}{27\chi}\frac{1+(5+\nu)\gamma/Y_{2D}}{B_m}. \tag{38}$$

Interestingly, θ_w is universal and given by $\cos^2\theta_w = 5/9$ for purely elastic capsules ($\gamma/Y_{2D} = 0$), i.e., it does not depend on the magnetic field or capsule elongation. This is also the limiting result for large values of $B_m/[1+(5+\nu)\gamma/Y_{2D}]$ (see Fig. 10). We note, however, that linear response theory is only applicable if $B_m/[1+(5+\nu)\gamma/Y_{2D}] \ll \chi Y_{2D}/\gamma$. For small magnetic fields, the results for θ_w from the linear response prediction (38) agree well with numerical results, as Fig. 10 shows.

Now we address the extent of the wrinkled region beyond linear response and calculate numerically the relative extent of the wrinkled region, L_w/L. A value $L_w/L = 0$ means that there are no wrinkles, while $L_w/L = 1$ describes a system where wrinkles extend from pole to pole. In Fig. 11 we change B_m and calculate L_w/L for different values of the capsule elongation a/b in the spheroidal shape, i.e., for $a/b < 5$. We use $\chi = 21$ and consider several values of the elastic parameter Y_{2D}/γ.

As Fig. 11 shows, there are no wrinkles for thin stretchable capsules, i.e., wrinkles only occur above a critical value of the dimensionless elastic parameter for

$$\frac{Y_{2D}}{\gamma} > 8.93 \quad \text{for } \chi = 21. \tag{39}$$

This result is only very weakly dependent on χ: We find $Y_{2D}/\gamma > 9.03$ for $\chi = 1$ and $Y_{2D}/\gamma > 8.87$ for $\chi = 100$. For small Y_{2D}, wrinkles are energetically unfavorable, i.e., the reduction of stretching energy E_{el} by wrinkles is smaller than the increase of E_γ due to the increase of the surface area. Slightly above the critical value (39), wrinkles can only occur for capsules with elongations $a/b \simeq 2.4$. Further increasing Y_{2D} (or shell thickness), the wrinkles become longer and appear for a wider range of elongations. The extent of wrinkling is still limited by two effects. At the lower elongation

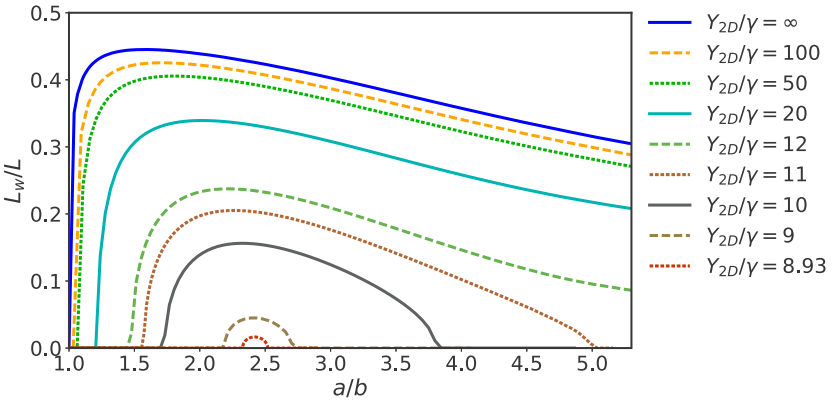

FIG. 11. Relative wrinkle length L_w/L as a function of elongation a/b for spheroidal capsules with fixed $\chi = 21$ and different values of Y_{2D}/γ. There are no wrinkles ($L_w/L = 0$) for $Y_{2D}/\gamma \lesssim 8.93$. The range of $L_w/L > 0$ and the extent of wrinkles increase with Y_{2D}/γ until they converge to an asymptotic curve for thick shells.

a/b, where $L_w/L = 0$, a certain elongation is needed to create a sufficient compressional stress at the equator to overcome the surface tension. The upper elongation a/b, where $L_w/L = 0$, is the point where the capsule is elongated so much that the transverse strain, which is related to Poisson's number ν and tends to shrink the capsule in the circumferential direction, counteracts any energy gain by the wrinkles. The wrinkles' length L_w/L for different elongations a/b turn out to be almost independent of the susceptibility χ.

In systems completely dominated by the elasticity and with negligible surface tension, there are wrinkles for almost all elongations. The wrinkle length quickly rises to a maximum and then slowly decreases due to the transverse strain.

V. DISCUSSION AND CONCLUSION

Magnetic or electric fields provide an interesting and fairly easily realizable route to the manipulation of elastic capsules if capsules can be filled with ferrofluids or dielectric substances. In this work we investigated the deformation of ferrofluid-filled capsules with thin elastic shells in uniform external magnetic fields numerically and using several analytic approaches. Our results apply unchanged to elastic capsules filled with a dielectric liquid in an external uniform electric field (see Sec. II B 3).

Numerically, we obtained equilibrium shapes by solving the coupled elastic and the magnetostatic problems in an iterative manner. To calculate the magnetic field, we used a combination of the finite element method and the boundary element method for a given capsule shape. The elastic capsule was described by nonlinear shell theory with a Hookean elastic law. By neglecting the bending rigidity we had to solve a system of four shape equations describing the force equilibrium in the absence of wrinkling and modified shape equations to take the effect of wrinkling into account. In addition to the dimensionless control parameters, the magnetic Bond number B_m and susceptibility χ, that characterize ferrofluid drops, we used the dimensionless ratio Y_{2D}/γ as an elastic control parameter.

As for ferrofluid droplets, we found spheroidal shapes at small and moderate magnetic fields, conical shapes at high magnetic fields, and a discontinuous shape transition between spheroidal and conical shapes. The general behavior of ferrofluid-filled capsules is comparable to drops but higher Bond numbers B_m are needed to reach the same elongation due to the additional elastic forces.

For small fields, the capsule shape is exactly spheroidal and its elongation is very well described by a linear response theory, which is in good agreement with our numerical results (see Fig. 4). The small field regime is easily accessible in experiments and our result (25) for the elongation a/b can

be used to determine the Young modulus Y_{2D} of the capsule material from elongation measurements if the magnetic properties of the ferrofluid are known. Also at moderate magnetic fields, capsule shapes with elongations $a/b \lesssim 3$ are prolate spheroids to a very good approximation and can be well described by an approximative energy minimization, as Fig. 7 shows.

For high fields a conical shape is possible. Capsules in a conical shape must have finite isotropic tensions and diverging isotropic stretches at the conical tip [see Eq. (29)] with a divergence exponent, which is given by the half opening angle α of the conical tip [see Eqs. (30) and (C4)]. The finiteness of tensions at the tip is a consequence of the nonlinear constitutive relations (13). An important consequence of the divergence of stretches at the tips of a conical shapes is that conical shapes are probably not observable experimentally because the high stretch factors give rise to rupture close to the capsule tips. Another consequence of such high stretch factors is that the nonlinear Hookean material law will become locally invalid. A real elastic capsule material will show plastic behavior for high stretches, followed by strain hardening and finally the material's destruction [78]. Our results can explain experimental observations of rupture of capsules filled with a dielectric liquid in external electric fields, where the capsules' shells were destroyed near the tip [21]. Then the existence of the sharp discontinuous shape transition into a conical shape can provide an interesting tool to trigger capsule rupture at rather well-defined magnetic (for ferrofluid-filled capsules) or electric (for dielectric-filled capsules) field values in future applications of such capsules as delivery systems.

Capsule rupture at the tips has some analogies with the disintegration of droplets in electric fields by emitting fluid jets at the tip [43,44]. Real fluid drops, which are not perfect conductors or perfect insulators, disintegrate at higher external electric fields by emitting jets of fluid at the tip. This is known from experiments [39] as well as quite precisely understood in theory [43,44]. In our setup of a fluid inside an elastic shell, the emission of a fluid jet is prevented by the shell at first. However, the tangential stresses at the tip that lead to the formation of a fluid jet may support the destruction of the shell near the tip. Once the shell is broken, a jet can be emitted. The rupture process itself cannot be described by our numerical approach and is an interesting topic for future work. Our elastic shape equation approach provides a very precise tool to solve the static elastic part of the problem, as long as nonlinear Hookean elasticity can be used. Also the generalization to other material laws, which are more appropriate for large strains, is possible [79]. Breaking of axisymmetry and topology changing rupture events cannot be easily incorporated into the shape equation approach, however. Also the magnetic field calculation should be improved if rupture is addressed, in particular in the capsule's tip region by using, for example, an elliptic mesh generation for the finite element method. One idea for a future improved simulation method that captures possible rupture processes at the tip is a dynamic simulation, where the magnetohydrodynamics of the fluid and the viscoelastic dynamics of the capsule shell including rupture processes can be calculated explicitly, similarly to what has been achieved for droplets in electric fields [43,44].

We presented a complete shape diagram in Fig. 7 and characterized the discontinuous shape transition between spheroidal and conical shapes. The slender-body theory predicts that this discontinuous shape transition only exists above the same critical value χ_c as for ferrofluid droplets, which was predicted to lie between $\chi_c \simeq 14.5$ [32] and $\chi_c \simeq 16.59$ [30]. It also predicts that χ_c is independent of the Young modulus Y_{2D} of the capsule. We predict that the critical χ_c will be very sensitive to the constitutive relation of the material. A strictly linear constitutive relation, for example, could give rise to diverging tensions at a conical tip, resulting in much higher values for χ_c.

We used the meridional stretch factor λ_s at the pole as a suitable order parameter to detect the spheroidal-conical transition, because stretches diverge at the tip of conical shapes but remain finite for spheroidal shapes, resulting in a pronounced jump of the stretch factor in the numerical calculations. The spheroidal-conical transition exhibits hysteresis effects in an interval $B_{m,c1} < B_m < B_{m,c2}$ between two critical Bond numbers, which are the limit of stability of the spheroidal and conical shapes. In the hysteresis interval both types of shapes are metastable. The interval has its maximum size for ferrofluid droplets and decreases slightly with increasing Young's modulus of the elastic shell. In the numerical calculations for $\chi = 21$, we observe hysteresis effects for all Y_{2D}/γ, which shows that, indeed, $\chi_c < 21$ for all the Young moduli.

It turned out that the formation of wrinkles is an important effect in systems with low surface tension γ. It has a visible effect on the elongation and the specific shape. Wrinkles appear for the first time for $Y_{2D}/\gamma \gtrsim 8.93$ (for $\chi = 21$) and are almost always present for systems with lower surface tension, even at very low elongations. Using this knowledge, it is possible to determine, for example, Y_{2D}/γ in experiments by a simple measurement of the wrinkle length L_w, which should be easy to perform in practice.

APPENDIX A: LINEAR RESPONSE AT SMALL MAGNETIC FIELDS

In this Appendix we derive the linear response of the capsule elongation a/b for small applied magnetic fields. Without applied field, the capsule is spherical with a rest radius R_0. In the presence of a surface tension γ, this also requires an internal pressure $p_0 = 2\gamma/R_0$ (Laplace-Young equation). If a small magnetic field is applied the additional position-dependent normal magnetic force density $f_m = O(H^2)$ [see Eq. (3)] acts on the spherical surface, resulting in normal displacements $u_R(\theta)\mathbf{e}_R$ and tangential displacements $u_\theta(\theta)\mathbf{e}_\theta$, where we use spherical coordinates with the polar angle θ (i.e., $\theta = 0$ at the upper pole and $\theta = \pi/2$ at the equator) and the spherical coordinate unit vectors $\mathbf{e}_R$ and $\mathbf{e}_\theta$. Because of axisymmetry the displacements do not depend on the azimuthal angle φ and there is no displacement in direction $\mathbf{e}_\varphi$. The deformed capsule surface is parametrized as $\mathbf{r}(\theta,\varphi) = [R_0 + u_R(\theta)]\mathbf{e}_R(\theta,\varphi)$ using polar and azimuthal angles θ and φ.

The new equilibrium shape has small displacements $u_R, u_\theta = O(H^2)$ and fulfills force equilibrium in two independent directions on the surface. We will consider normal force equilibrium as described by the Laplace-Young equation [see Eq. (14)] and tangential force equilibrium [see Eq. (15)]. We start with the Laplace-Young equation

$$\kappa_s(\tau_s + \gamma) + \kappa_\varphi(\tau_\varphi + \gamma) = p_0 + f_m, \tag{A1}$$

where γ is a surface tension, τ_s and τ_φ are elastic tensions, and $f_m = (\mu_0\chi/2)[H^2 + \chi(\mathbf{n}\cdot\mathbf{H})^2]$ is the small normal magnetic force density (3) causing small displacements. The pressure will change to linear order in the displacements $p_0 = 2\gamma/R_0 + O(u_R,u_\theta)$ to ensure a fixed volume. In spherical coordinates and in linear order in the displacements, the stretch factors can be calculated using $r = \sqrt{g_{\varphi\varphi}} = |\partial_\varphi \mathbf{r}|$ ($r_0 = R_0 \sin\theta$) and $ds = \sqrt{g_{\theta\theta}}\, d\theta = |\partial_\theta \mathbf{r}| d\theta$ ($ds_0 = R_0 d\theta$):

$$\lambda_s = \frac{ds}{ds_0} = \frac{|\partial_\theta \mathbf{r}|}{R_0} = 1 + \frac{1}{R_0}(u_R + \partial_\theta u_\theta),$$
$$\lambda_\varphi = \frac{r}{r_0} = \frac{|\partial_\varphi \mathbf{r}|}{R_0 \sin\theta} = 1 + \frac{1}{R_0}(u_R + u_\theta \cot\theta).$$

In linear order in the displacements the constitutive relations (13) can then be written as [80]

$$\tau_\varphi - \nu\tau_s = Y_{2D}(\lambda_\varphi - 1) = \frac{Y_{2D}}{R_0}(u_\theta \cot\theta + u_R), \tag{A2}$$
$$\tau_s - \nu\tau_\varphi = Y_{2D}(\lambda_s - 1) = \frac{Y_{2D}}{R_0}(\partial_\theta u_\theta + u_R). \tag{A3}$$

Elastic tensions are small for small magnetic fields, $\tau_s, \tau_\varphi = O(u_R,u_\theta) = O(H^2)$, whereas the fluid surface tension γ cannot be considered small. Therefore, we also need to consider curvature corrections up to linear order $O(u_R,u_\theta)$ in Eq. (A1):

$$\kappa_s + \kappa_\varphi \approx \frac{2}{R_0} - \frac{1}{R_0^2}\left(2u_R - \partial_\theta^2 u_R + \partial_\theta u_R \cot\theta\right).$$

On the right-hand side of Eq. (A1), we can use $\mathbf{n} = \mathbf{e}_R$ for the outward unit normal to $O(H^2)$. This results in the following normal force balance to linear order in the displacements, i.e., to $O(H^2)$:

$$\begin{aligned} &-\gamma\left(2u_R - \partial_\theta^2 u_R + \partial_\theta u_R \cot\theta\right) + R_0(\tau_s + \tau_\varphi) \\ &\quad = \left(p_0 R_0^2 - 2R_0\gamma\right) + \frac{\mu_0}{2}\chi H^2 R_0^2(1 + \chi\cos^2\theta). \end{aligned} \tag{A4}$$

We first solve this equation for a ferrofluid droplet ($Y_{2D}/\gamma = 0$), where the elastic stresses and thus u_θ are zero. Boundary conditions are $\partial_\theta u_R(0) = \partial_\theta u_R(\pi/2) = 0$ and $u_\theta(0) = u_\theta(\pi/2) = 0$ to avoid kinks (we are not considering conical shapes in the linear response) or holes in the shape. Then $u_\theta = 0$ and an ansatz

$$u_R = A + B\cos^2\theta \tag{A5}$$

leads to a solution

$$B = \frac{\mu_0}{8\gamma}\chi^2 H^2 R_0^2 \approx \frac{9\mu_0\chi^2}{8\gamma(3+\chi)^2} H_0^2 R_0^2, \tag{A6}$$

$$A = -\frac{1}{2}\left(\frac{p_0 R_0}{\gamma} - 2\right)R_0 - \frac{\mu_0}{4\gamma}\chi\left(1 + \frac{\chi}{2}\right)H^2 R_0^2. \tag{A7}$$

To leading order in $u_R = O(H^2)$, the ansatz (A5) describes a spheroid such that we can replace the magnetic field H in Eq. (A6) by the analytically known value for a field inside a spheroid [70],

$$H = H_0/(1 + n\chi), \tag{A8}$$

where n denotes the demagnetization factor. To leading order $O(H^2)$ it is also correct to use the result $n = 1/3$ for a sphere (A8). Moreover, volume conservation requires

$$A = -B/3, \tag{A9}$$

which determines the pressure correction $p_0 = 2\gamma/R_0 + O(H^2)$ from Eq. (A7). For the deformation a/b we find, to leading order in $u_R = O(H^2)$,

$$\frac{a}{b} = \frac{R_0 + u_R(0)}{R_0 + u_R(\pi/2)} \approx 1 + \frac{B}{R_0} = 1 + \frac{9\mu_0 R_0\chi^2}{8\gamma(3+\chi)^2}\chi H_0^2. \tag{A10}$$

For a ferrofluid-filled elastic capsule we also need to consider the force equilibrium in the tangential direction because the total tensions $\gamma + \tau_s \neq \gamma + \tau_\varphi$ become anisotropic now (for a liquid interface with $\tau_s = \tau_\varphi = 0$ the force equilibrium in tangential direction becomes exactly equivalent to the normal force equilibrium, i.e., the Laplace-Young equation). The tangential force equilibrium (15) can be written as

$$\tau_\varphi = \partial_r(r\tau_s) = \tau_s + r\partial_r\tau_s = \tau_s + \frac{\partial_\theta\tau_s}{\partial_\theta r}.$$

Using $r = |\partial_\varphi \mathbf{r}| = \sin\theta(R_0 + u_R + u_\theta\cot\theta)$ and Eq. (A3) for the elastic stresses, the tangential force equilibrium becomes

$$\begin{aligned} \tau_\varphi - \tau_s &= \frac{Y_{2D}}{(1+\nu)R_0}(u_\theta\cot\theta - \partial_\theta u_\theta) \\ &= \partial_r\tau_s = \frac{Y_{2D}}{(1-\nu^2)R_0}\left(\tan\theta\,\partial_\theta^2 u_\theta + \nu\partial_\theta u_\theta - \frac{\nu u_\theta}{\cos\theta\sin\theta} + (1-\nu)\tan\theta\,\partial_\theta u_R\right). \end{aligned} \tag{A11}$$

For the ferrofluid capsule, the two force equilibria (A4), where τ_s and τ_φ have to be expressed in terms of the displacements using the constitutive relations (A3),

$$\tau_s + \tau_\varphi = \frac{Y_{2D}}{(1-\nu)R_0}(2u_R + u_\theta\cot\theta + \partial_\theta u_\theta),$$

and Eq. (A11) have to be solved for the deformed capsule shape. Boundary conditions are $\partial_\theta u_R(0) = \partial_\theta u_R(\pi/2) = 0$ and $u_\theta(0) = u_\theta(\pi/2) = 0$. For the fluid limit $Y_{2D}/\gamma = 0$, we derived an exact solution above. For the ferrofluid capsule, we make an ansatz

$$u_R = A + B\cos^2\theta, \quad u_\theta = C\sin\theta\cos\theta, \tag{A12}$$

which still describes a spheroid to leading order in the displacements because $u_\theta \neq 0$ only generates an additional tangential displacement. Then the tangential force equilibrium gives

$$C = -\frac{2(1+\nu)}{5+\nu}B. \tag{A13}$$

For the ferrofluid capsule, the normal force equilibrium (A4) gives

$$B = \frac{\mu_0(5+\nu)}{8[Y_{2D}+(5+\nu)\gamma]}\chi^2 H^2 R_0^2, \tag{A14}$$

$$A = \frac{1-\nu}{2}\left(\frac{p_0 R_0}{Y_{2D}} - 2\frac{\gamma}{Y_{2D}}\right)R_0 + \frac{\mu_0}{4(1-\nu)Y_{2D}}\chi H^2 R_0^2\left(1+\frac{\chi}{2}\right) - \frac{C}{1+\nu} \tag{A15}$$

and the relation $A = -B/3$ [see Eq. (A9)] from the fixed volume constraint determines the pressure p_0. For the deformation a/b we find, to leading order in $u_R = O(H^2)$,

$$\frac{a}{b} = \frac{R_0 + u_R(0)}{R_0 + u_R(\pi/2)} \approx 1 + \frac{B}{R_0} = 1 + \frac{9\mu_0 R_0 \chi^2(5+\nu)}{8[Y_{2D}+\gamma(5+\nu)](3+\chi)^2}H_0^2. \tag{A16}$$

The criterion for wrinkling is $\tau_\varphi + \gamma < 0$, where

$$\tau_\varphi = \frac{Y_{2D}}{(1-\nu^2)R_0}[u_\theta\cot\theta + (1+\nu)u_R + \nu\partial_\theta u_\theta] \approx B\frac{1-\nu^2}{5+\nu}\left(-\frac{5}{3} + 3\cos^2\theta\right) \tag{A17}$$

from Eq. (A3) and using Eq. (A12) with Eqs. (A13) and (A9).

APPENDIX B: APPROXIMATIVE ENERGY MINIMIZATION FOR SPHEROIDAL SHAPES

In this Appendix we derive an analytical approximation for the elongation a/b of the capsule at moderate magnetic forces by minimizing an approximative total energy, which assumes a spheroidal shape for magnetic and elastic contributions and constant elastic stretch factors throughout the shell. We minimize the total energy, the sum of surface, magnetic, and elastic energies with respect to the inverse elongation ratio $k \equiv b/a < 1$ at fixed volume $V = (4\pi/3)ab^2 = V_0$ (quantities $\cdots|_V$ are at fixed volume V):

$$0 = \frac{dE_\gamma|_V}{dk} + \frac{dE_{\mathrm{mag}}|_V}{dk} + \frac{dE_{\mathrm{el}}|_V}{dk}.$$

For fixed volume $V = (4\pi/3)ab^2 = (4\pi/3)R_0^2 = V_0$ we have

$$a|_V = R_0 k^{-2/3}, \quad b|_V = R_0 k^{1/3}.$$

The surface energy (26), which is proportional to the surface area A at fixed volume, can then be written as

$$E_\gamma|_V = \gamma A|_V \quad \text{with } A|_V = A_0\frac{1}{2}k^{-1/3}\left(k + \frac{1}{\epsilon}\arcsin\epsilon\right),$$

where $\epsilon = \epsilon(k) \equiv \sqrt{1-k^2}$ is the spheroid's eccentricity and $A_0 = 4\pi R_0^2$ the area of the undeformed sphere. The magnetic energy (27) is given as

$$E_{\mathrm{mag}}|_V = -\frac{V_0\mu_0}{2}\frac{\chi}{1+n\chi}H_0^2 = -\gamma A_0 B_m \frac{1}{3(1+n\chi)},$$

where n is the demagnetization factor

$$n = n(k) = \frac{k^2}{2\epsilon^3(k)}\left(-2\epsilon(k) + \ln\frac{1+\epsilon(k)}{1-\epsilon(k)}\right)$$

and $B_m = \mu_0 R_0 \chi H_0^2/2\gamma$ is the Bond number. Finally, we calculate the elastic stretch energy (28) via

$$E_{\mathrm{el}}|_V = A_0 \frac{Y_{2\mathrm{D}}}{2(1-\nu^2)}[(e_s|_V)^2 + 2\nu e_s|_V e_\varphi|_V + (e_\varphi|_V)^2]$$

using the approximation of constant e_s and e_φ. At fixed volume, we find

$$\begin{aligned} e_s &= \frac{P_{\mathrm{ellipse}}}{P_{\mathrm{circle}}} - 1 \approx \frac{a+b}{2R_0}\left(1 + \frac{3\eta^2}{10+\sqrt{4-3\eta^2}}\right) - 1, \\ e_s|_V &= \frac{k^{-2/3}(1+k)}{2}\left(1 + \frac{3\eta^2(k)}{10+\sqrt{4-3\eta^2(k)}}\right) - 1, \\ e_\varphi &= \frac{b}{R_0} - 1, \quad e_\varphi|_V = k^{1/3} - 1, \end{aligned}$$

with $\eta = \eta(k) \equiv (b-a)/(b+a) = (k-1)/(k+1)$.

Now we can find the elongation k that minimizes the total energy at fixed volume; k can only be determined implicitly as a function of the magnetic field H_0 by the following relation between the Bond number $B_m = \mu_0 R_0 \chi H_0^2/2\gamma$ and a complicated function $g(k)$ of the elongation k, which also depends on the susceptibility χ, the dimensionless Young modulus $Y_{2\mathrm{D}}/\gamma$, and Poisson's ratio ν:

$$B_m = \frac{\mu_0 R_0 \chi H_0^2}{2\gamma} = g(k)$$

with

$$g(k) \equiv -3\left(\frac{1}{\chi} + n(k)\right)^2 \chi \frac{c_1(k) + \frac{Y_{2\mathrm{D}}}{2\gamma(1-\nu^2)} c_2(k,\nu)}{c_3(k)}, \tag{B1}$$

where

$$\begin{aligned} c_1(k) &\equiv \frac{1}{A_0}\frac{dA|_V}{dk}, \\ c_2(k,\nu) &\equiv \left[2e_s|_V \frac{de_s|_V}{dk} + 2\nu\left(e_\varphi|_V \frac{de_s|_V}{dk} + e_s|_V \frac{de_\varphi|_V}{dk}\right) + 2e_\varphi|_V \frac{de_\varphi|_V}{dk}\right], \\ c_3(k) &\equiv \frac{dn}{dk} = \frac{-3k}{\epsilon^4(k)} + \left(\frac{k}{\epsilon^3(k)} + \frac{3k^3}{2\epsilon^5(k)}\right)\ln\frac{1+\epsilon(k)}{1-\epsilon(k)}. \end{aligned}$$

The functions $c_1(k)$ and $c_3(k)$ from surface and magnetic energies depend on the inverse elongation ration $k = b/a < 1$ only, whereas the function $c_2(k,\nu)$ from the elastic energy also depends on Poisson's ratio ν (which is set to $\nu = 1/2$ and thus fixed throughout this paper). This relation reduces to the results of Bacri and Salin [27] for ferrofluid droplets in the limit $Y_{2\mathrm{D}} = 0$, where the function $c_2(k,\nu)$ drops from Eq. (B1). The solid lines in Fig. 7 show plots of $1/k = a/b$ versus B_m as given by the relation $B_m = g(k)$.

APPENDIX C: CONICAL SHAPES FOR ELASTIC MEMBRANES WITH SPHERICAL REST SHAPE

1. Stretches and tensions at a conical tip with normal magnetic forces

In this Appendix we show that a conical shape, as it is observed for ferrofluid drops at a critical field strength, is also possible for an elastic capsule with a spherical rest shape and stretched by normal magnetic forces but requires diverging and asymptotically isotropic stretches with an exponent determined by the opening angle of the cone, whereas elastic tension have to remain finite and isotropic at the tip of the cone. A sharp conical tip implies a nonzero slope angle $\psi(s_0 = 0) > 0$, where $\alpha = \pi/2 - \psi(0)$ is half of the opening angle of the cone. In contrast to a ferrofluid droplet with constant and isotropic surface tension γ, an elastic capsule develops additional elastic tensions τ_s and τ_φ, which depend on the state of stretching, i.e., the stretches λ_s and λ_φ with respect to the spherical rest shape via the nonlinear constitutive relations (13), and which have to fulfill an additional tangential force equilibrium (15) that we rewrite as

$$\tau_\varphi = \partial_r(r\tau_s) = \tau_s + r\partial_r\tau_s. \tag{C1}$$

It is important to note that the tangential force equilibrium does not contain external magnetic forces, which are always normal to the surface [see Eqs. (16) and (14)]. The internal tangential force equilibrium has to be compatible with the deformation into a conical tip.

First we show that $\tau_s(0)$ and $\tau_\varphi(0)$ have to remain finite at the tip at $s_0 = 0$ (corresponding to $r = 0$). The reason for a divergence of one of the tensions can only be a divergence of one or both of the stretches. According to the nonlinear constitutive relations (13), only one of the tensions can exhibit a divergence ($\lambda_s/\lambda_\varphi$ and $\lambda_\varphi/\lambda_s$ cannot both diverge). Then it is easy to verify that a single divergent tension at $r = 0$ contradicts the force equilibrium (C1). Therefore, both tensions have to remain finite at $s_0 = 0$ (or $r = 0$).

Next we show that finiteness of the tensions at the conical tip necessarily leads to tension isotropy $\tau_s(0) = \tau_\varphi(0)$ at the tip. Because magnetic forces are stretching forces, both tensions are equal and stretching, $\tau_s(0) = \tau_\varphi(0) > 0$. If $\tau_s(0) \neq \tau_\varphi(0)$, the tangential force equilibrium (C1) immediately leads to $\partial_r\tau_s \approx [\tau_\varphi(0) - \tau_s(0)]/r$ for small r, resulting in a logarithmically diverging $\tau_s \propto -\ln r$ for small r contradicting finiteness.

The equality $\tau_s(0) = \tau_\varphi(0)$ at the tip also leads to isotropy of the stretches $\lambda_s(0) = \lambda_\varphi(0)$ at the tip because of the constitutive relations (13), however, not necessarily to finiteness of the stretches at the tip. Therefore, we have to discuss the cases of finite and diverging stretches $\lambda_s = \lambda_\varphi$ at the conical tip separately.

We start with finite isotropic stretches $\lambda_s(0) = \lambda_\varphi(0) < \infty$. Then we can apply l'Hôpital's rule at the tip $s_0 = 0$:

$$\lambda_\varphi(0) = \lim_{s_0\to 0}\frac{r}{r_0} = \lim_{s_0\to 0}\frac{r'}{r_0'} = \frac{\lambda_s\cos[\psi(0)]}{\cos[\psi_0(0)]} = \lambda_s(0)\cos[\psi(0)] \tag{C2}$$

[where we used $\psi_0(0) = 0$ for the spherical rest shape]. Equality of the stretches $\lambda_s(0) = \lambda_\varphi(0)$ then leads to the conclusion $\psi(0) = 0$, i.e., a sharp conical tip is impossible if stretches remain finite at the tip.

L'Hôpital's rule can no longer be applied if the stretches diverge at the tip (remaining asymptotically isotropic), i.e.,

$$\lambda_s(s_0) \approx \lambda_\varphi(s_0) \approx \text{const}s_0^{-\beta} \tag{C3}$$

for $s_0 \approx 0$ with an exponent $\beta > 0$. Because of $\lambda_s = r'/\cos\psi$, this requires $r(s_0) \approx \text{const}s_0^{1-\beta}/(1-\beta)\cos\psi(0)$ for $s_0 \approx 0$, whereas $r_0(s_0) = R_0\sin(s_0/R_0) \approx s_0$ for the spherical rest shape. Then

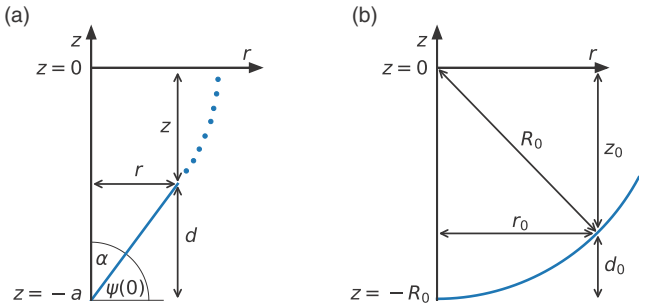

FIG. 12. Illustration of the geometry at the capsule's south pole (not true to scale) for (a) a conical tip and (b) the spheroidal reference shape.

Eq. (C2) is replaced by

$$\lambda_\varphi(s_0) = \lim_{s_0\to 0}\frac{r}{r_0} = \frac{\text{const} s_0^{-\beta}}{(1-\beta)\cos\psi(0)} = \lim_{s_0\to 0}\frac{1}{1-\beta}\frac{r'}{r_0'} = \lambda_s(s_0)\frac{\cos[\psi(0)]}{1-\beta}$$

for $s_0 \approx 0$. The equality $\lambda_s(s_0) \approx \lambda_\varphi(s_0)$ necessarily leads to the condition

$$\beta = \cos[\psi(0)] - 1 = \sin\alpha - 1 \tag{C4}$$

between the exponent β of the divergent stretches and the half opening angle $\alpha = \pi/2 - \psi(0)$ of the conical tip.

In conclusion, a deformation of the spherical rest shape into a sharp conical tip with $\psi(0) > 0$ is only possible if stretches are asymptotically isotropic and diverge as $\lambda_s(s_0) \approx \lambda_\varphi(s_0) \sim s_0^{-\beta}$ with an exponent β, which is related by Eq. (C4) to the opening angle 2α of the cone. Because of the nonlinear constitutive relation (13), diverging and isotropic stretches are compatible with finite and isotropic tensions at the tip with

$$\tau_s(0) = \tau_\varphi(0) = \frac{Y_{2D}}{1-\nu}. \tag{C5}$$

Note that away from the tip ($s_0 > 0$), tensions and stretches feature anisotropic corrections.

2. Governing equations for stretches and tensions in a conical shape with spherical rest shape

In this section we present how to systematically calculate stretches and elastic tensions in a deformation from a spherical rest shape into a conical shape by deriving the governing equations. This is the basis of the generalization of the slender-body theory of Stone *et al.* from ferrofluid conical droplets to capsules.

We assume that the conical shape is given by a function $r(z)$, where z runs from the bottom of the cone at $z = -a$ to its top at $z = a$. We will show that, if the conical shape $r(z)$ is known, we can calculate all stretches and tensions in this shape. The rest shape is spherical and parametrized analogously by a function $r_0(z_0) = (R_0^2 - z_0^2)^{1/2}$ with $z_0 \in [-R_0, R_0]$. For the following it is advantageous to replace z and z_0 by coordinates $d = a + z$ measuring the distance from the lower conical tip and $d_0 = R_0 + z_0$ measuring the distance from the corresponding south pole of the sphere. This geometry is illustrated in Fig. 12.

Given a conical shape $r(d)$ and the spherical rest shape

$$r_0(d_0) = \left(2R_0 d_0 - d_0^2\right)^{1/2}, \tag{C6}$$

we want to show how the function $d(d_0)$ describing the stretching in the z direction can be calculated systematically from the tangential force equilibrium (C1) or (15) and the constitutive relations (13).

If the conical shape $r(d)$ and the function $d(d_0)$ are given [and the spherical rest shape $r_0(d_0)$] the meridional and hoop stretches can be calculated as a function of d_0 by

$$\lambda_\varphi = \frac{r(d(d_0))}{r_0(d_0)} = \frac{r(d(d_0))}{\left(2R_0d_0 - d_0^2\right)^{1/2}},$$
$$\lambda_s = \frac{ds}{ds_0} = \frac{[1 + r'(d(d_0))^2]^{1/2}}{[1 + r_0'(d_0)^2]^{1/2}} d'(d_0) = [1 + r'(d(d_0))^2]^{1/2} \frac{\left(2R_0d_0 - d_0^2\right)^{1/2}}{R_0} d'(d_0), \tag{C7}$$

where $\lambda_z \equiv d'(d_0) = dz/dz_0$ is the stretch in the z direction.

If both stretches are known then the constitutive relations (13) can be used to express tensions τ_s and τ_φ as algebraic functions of the stretches λ_s and λ_φ from Eq. (C7) and thus as functions of d_0, the conical shape $r(d)$, and the unknown function $d(d_0)$ and its derivative. These tensions have to fulfill the tangential force equilibrium (C1), which we rewrite in terms of stretches using the constitutive relations (13),

$$\tau_\varphi = \tau_s + r\,\partial_r \tau_s,$$
$$\lambda_\varphi^3 - (1+\nu)\lambda_\varphi^2 = \lambda_s^2\lambda_\varphi - (1+\nu)\lambda_s\lambda_\varphi + r\lambda_s\{\lambda_\varphi(\partial_r\lambda_s) - (\partial_r\lambda_\varphi)[\lambda_s - (1+\nu)]\}. \tag{C8}$$

Plugging in the stretches from (C7) and using

$$\partial_r = \frac{1}{\partial_{d_0} r}\partial_{d_0} = \frac{1}{r'(d(d_0))d'(d_0)}\partial_{d_0},$$

we obtain a complicated nonlinear differential equation for the unknown function $d(d_0)$ and its derivative $\lambda_z(d_0) = d'(d_0)$. If this differential equation can be solved, all stretches and tensions arising from the deformation from $r_0(d_0)$ into $r(d)$ are determined, in principle. Unfortunately, this equation cannot be solved in general. In the next section we obtain features of a solution close to the conical tip.

3. Stretches and tensions in the vicinity of a conical tip for a spherical rest shape

In the vicinity of a the conical tip the conical shape $r(d)$ with a half opening angle α becomes strictly conical and we can use

$$r(d) = d\tan\alpha, \tag{C9}$$

resulting in stretches

$$\lambda_\varphi = \frac{\tan\alpha}{\left(2R_0d_0 - d_0^2\right)^{1/2}} d(d_0),$$
$$\lambda_s = \frac{1}{\cos\alpha}\frac{\left(2R_0d_0 - d_0^2\right)^{1/2}}{R_0} d'(d_0). \tag{C10}$$

Close to the conical tip, λ_s and λ_φ are diverging and asymptotically equal according to Appendix C 1. Requiring $\lambda_s = \lambda_\varphi$ for small d_0 gives a differential equation

$$d'(d_0) = \sin\alpha \frac{R_0}{2R_0d_0 - d_0^2} d(d_0), \tag{C11}$$

which is solved by

$$d(d_0) = a\left(\frac{d_0}{2R_0 - d_0}\right)^{(\sin\alpha)/2} \approx a\left(\frac{d_0}{2R_0}\right)^{(\sin\alpha)/2} \propto d_0^{(\sin\alpha)/2},$$

where we use a boundary condition $d(R_0) = a$ resulting from the conservation of the mirror symmetry plane at $z = z_0 = 0$. This results in

$$r(d(d_0)) = \tan\alpha[d(d_0)] \approx a\tan\alpha\left(\frac{d_0}{2R_0}\right)^{(\sin\alpha)/2}$$

and, using (C10),

$$\lambda_s = \lambda_\varphi \approx \frac{a}{2R_0}\tan\alpha\left(\frac{d_0}{2R_0}\right)^{(\sin\alpha-1)/2} = \frac{a\tan\alpha}{2R_0}\left(\frac{r}{a\tan\alpha}\right)^{1-1/\sin\alpha}. \tag{C12}$$

Noting that $d_0 \approx R_0[1-\cos(s_0/R_0)] \approx s_0^2/2R_0$ for the spherical rest shape, the exponent in Eq. (C12) is exactly equivalent to our above result (C4), $\beta = 1-\sin\alpha$, for the relation between the exponent β of the divergent stretches $\lambda_s(s_0) \approx \lambda_\varphi(s_0) \approx s_0^{-\beta}$ and the half opening angle α of the conical tip.

Away from the tip, the stretches and tensions acquire anisotropic corrections. Therefore, we start with an ansatz

$$\begin{aligned}\lambda_s &= br^{-\tilde\beta} + b_s r^{-\gamma}, \quad \lambda_\varphi = br^{-\tilde\beta} + b_\varphi r^{-\gamma},\\ \tilde\beta &= 1/\sin\alpha - 1, \quad b \approx (a\tan\alpha)^{1+\tilde\beta}/2R_0\end{aligned} \tag{C13}$$

for small r in the vicinity of the conical tip, where $\gamma < \tilde\beta$. We use this ansatz in the tangential force balance relation (C8) derived in Appendix C 2. First we obtain the tensions, which are isotropic and in agreement with (C5) to leading order but also acquire anisotropic corrections

$$\begin{aligned}\tau_s\frac{1-\nu^2}{Y_{2D}} &= 1+\nu + \frac{b_s-b_\varphi}{b}r^{\tilde\beta-\gamma} - \frac{1+\nu}{b}r^{\tilde\beta} + \frac{(1+\nu)b_s}{b^2}r^{2\tilde\beta-\gamma} - \frac{b_\varphi(b_s+b_\varphi)}{b^2}r^{2\tilde\beta-2\gamma},\\ \tau_\varphi\frac{1-\nu^2}{Y_{2D}} &= 1+\nu + \frac{b_\varphi-b_s}{b}r^{\tilde\beta-\gamma} - \frac{1+\nu}{b}r^{\tilde\beta} + \frac{(1+\nu)b_\varphi}{b^2}r^{2\tilde\beta-\gamma} - \frac{b_s(b_s+b_\varphi)}{b^2}r^{2\tilde\beta-2\gamma},\end{aligned}$$

neglecting terms $O(r^{3\tilde\beta-2\gamma})$. These expression are used in the tangential force balance relation (C8), $\tau_\varphi - \tau_s = r\partial_r\tau_s$, in which we compare coefficients order by order in r in order to determine the exponent γ and the coefficients b_s and b_φ.

If we assume $\gamma > 0$ the leading-order terms are $O(r^{\tilde\beta-\gamma})$, and comparing coefficients gives a contradictory relation $2 = \gamma - \tilde\beta < 0$. It follows that

$$\gamma = 0,$$

i.e., the leading anisotropic corrections in the stretches (C13) are constant.

Continuing with $\gamma = 0$, terms $O(r^{\tilde\beta-\gamma})$ and $O(r^{\tilde\beta})$ are of equal order and comparing all coefficients gives

$$b_s - b_\varphi = \frac{\tilde\beta(1+\nu)}{2+\tilde\beta} > 0,$$

i.e., the anisotropy close to the tip is such that $\lambda_s > \lambda_\varphi$ and $\tau_s > \tau_\varphi$. For the tensions this results in

$$\tau_s = \frac{Y_{2D}}{1-\nu}\left(1 - \frac{1}{b}\frac{1}{1+\tilde\beta/2}r^{\tilde\beta}\right), \quad \tau_\varphi = \frac{Y_{2D}}{1-\nu}\left(1 - \frac{1}{b}\frac{1}{1+\tilde\beta}r^{\tilde\beta}\right), \tag{C14}$$

which specifies the leading anisotropic corrections to Eq. (C5). Finally, we can compare coefficients of all terms $O(r^{2\tilde\beta})$ for $\gamma = 0$ to obtain

$$b_\varphi^2 - b_s^2 + (1+\nu)(b_\varphi - b_s) = 2\tilde\beta(1+\nu)b_s - 2\tilde\beta b_\varphi(b_s+b_\varphi)$$

which can be used to go on and determine both b_s and b_φ if needed.

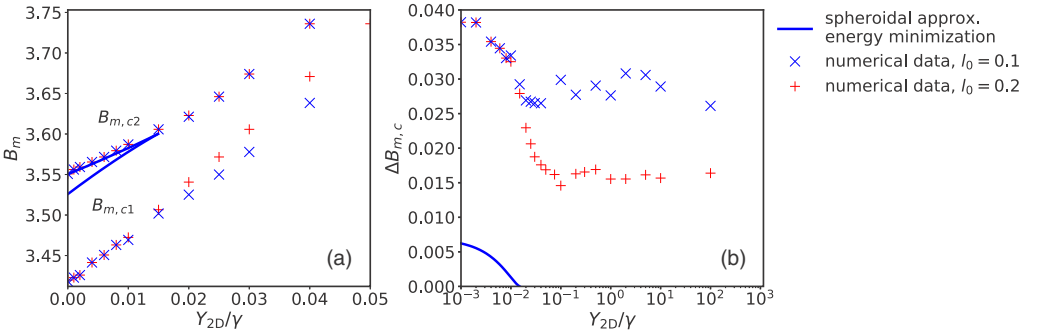

FIG. 13. Comparison of data from Fig. 9 for $l_0 = 0.1$ (blue) with data for $l_0 = 0.2$ (red). There is an increasing deviation for higher values of Y_{2D}/γ.

APPENDIX D: DISCRETIZATION ERRORS

To observe the transition to a conical shape, it is necessary to have a high resolution for the finite element–boundary element method in the tip of the capsule. If we consider the number of boundary elements to be fixed to $N = 250$, we can vary the density of elements near the tip by changing the parameter l_0 [see Sec. II B 2 and Eq. (7)]. For different values of l_0, we see a quite different numerical behavior. Every result in the text above is calculated with $l_0 = 0.1$. For significantly smaller values of l_0, we cannot calculate conical shapes. The problem is that our shooting method for the elastic shape equations does not find solutions anymore due to extremely high and rapidly changing stretch factors at the tip [$\lambda_s(s_0 = 0) > 10^4$]. On the other hand, with constant element density ($l_0 = 1$), a shape transition cannot be found anymore; the capsule's shape stays rounded. This indicates that the numerical calculation of the shape transition is prone to changes of l_0. An example of this phenomenon can be seen in Fig. 13, which is identical to Fig. 9 but with additional data for $l_0 = 0.2$. Lowering the elements' density at the tip leads to slightly different values for the critical Bond numbers and lowers the relative sizes of the hysteresis loops, especially for higher values of Y_{2D}/γ.

[1] M. P. Neubauer, M. Poehlmann, and A. Fery, Microcapsule mechanics: From stability to function, Adv. Colloid Interface Sci. **207**, 65 (2014).
[2] A. Fery, F. Dubreuil, and H. Möhwald, Mechanics of artificial microcapsules, New J. Phys. **6**, 18 (2004).
[3] O. I. Vinogradova, O. V. Lebedeva, and B.-S. Kim, Mechanical behavior and characterization of microcapsules, Annu. Rev. Mater. Res. **36**, 143 (2006).
[4] C. Gao, E. Donath, S. Moya, V. Dudnik, and H. Möhwald, Elasticity of hollow polyelectrolyte capsules prepared by the layer-by-layer technique, Eur. Phys. J. E **5**, 21 (2001).
[5] S. Sacanna, W. T. M. Irvine, L. Rossi, and D. J. Pine, Lock and key colloids through polymerization-induced buckling of monodisperse silicon oil droplets, Soft Matter **7**, 1631 (2011).
[6] S. S. Datta, S.-H. Kim, J. Paulose, A. Abbaspourrad, D. R. Nelson, and D. A. Weitz, Delayed Buckling and Guided Folding of Inhomogeneous Capsules, Phys. Rev. Lett. **109**, 134302 (2012).
[7] S. Knoche and J. Kierfeld, Buckling of spherical capsules, Phys. Rev. E **84**, 046608 (2011).
[8] S. Knoche and J. Kierfeld, The secondary buckling transition: Wrinkling of buckled spherical shells, Eur. Phys. J. E **37**, 62 (2014).
[9] S. Knoche and J. Kierfeld, Secondary polygonal instability of buckled spherical shells, Europhys. Lett. **106**, 24004 (2014).
[10] V. Jadhao, C. K. Thomas, and M. O. de la Cruz, Electrostatics-driven shape transitions in soft shells, Proc. Natl. Acad. Sci. USA **111**, 12673 (2014).

[11] H.-H. Boltz and J. Kierfeld, Shapes of sedimenting soft elastic capsules in a viscous fluid, Phys. Rev. E **92**, 033003 (2015).
[12] C. I. Zoldesi, I. L. Ivanovska, C. Quilliet, G. J. L. Wuite, and A. Imhof, Elastic properties of hollow colloidal particles, Phys. Rev. E **78**, 051401 (2008).
[13] D. Vella, A. Ajdari, A. Vaziri, and A. Boudaoud, The indentation of pressurized elastic shells: From polymeric capsules to yeast cells, J. R. Soc. Interface **9**, 448 (2012).
[14] H. Rehage, M. Husmann, and A. Walter, From two-dimensional model networks to microcapsules, Rheol. Acta **41**, 292 (2002).
[15] D. Vella, A. Ajdari, A. Vaziri, and A. Boudaoud, Wrinkling of Pressurized Elastic Shells, Phys. Rev. Lett. **107**, 174301 (2011).
[16] E. Aumaitre, S. Knoche, P. Cicuta, and D. Vella, Wrinkling in the deflation of elastic bubbles, Eur. Phys. J. E **36**, 22 (2013).
[17] S. Knoche, D. Vella, E. Aumaitre, P. Degen, H. Rehage, P. Cicuta, and J. Kierfeld, Elastometry of deflated capsules: Elastic moduli from shape and wrinkle analysis, Langmuir **29**, 12463 (2013).
[18] G. Pieper, H. Rehage, and D. Barthès-Biesel, Deformation of a capsule in a spinning drop apparatus, J. Colloid Interface Sci. **202**, 293 (1998).
[19] D. Barthès-Biesel, Modeling the motion of capsules in flow, Curr. Opin. Colloid Interface Sci. **16**, 3 (2011).
[20] P. Degen, S. Peschel, and H. Rehage, Stimulated aggregation, rotation, and deformation of magnetite-filled microcapsules in external magnetic fields, Colloid Polym. Sci. **286**, 865 (2008).
[21] R. B. Karyappa, S. D. Deshmukh, and R. M. Thaokar, Deformation of an elastic capsule in a uniform electric field, Phys. Fluids **26**, 122108 (2014).
[22] R. E. Rosenweig, *Ferrohydrodynamics* (Cambridge University Press, Cambridge, 1985).
[23] P. A. Voltairas, D. I. Fotiadis, and C. V. Massalas, Elastic stability of silicone ferrofluid internal tamponade (SFIT) in retinal detachment surgery, J. Magn. Magn. Mater. **225**, 248 (2001).
[24] D. L. Holligan, G. T. Gillies, and J. T. Dailey, Magnetic guidance of ferrofluidic nanoparticles in an in vitro model of intraocular retinal repair, Nanotechnology **14**, 661 (2003).
[25] X. Liu, M. D. Kaminski, J. S. Riffle, H. Chen, M. Torno, M. R. Finck, L. Taylor, and A. J. Rosengart, Preparation and characterization of biodegradable magnetic carriers by single emulsion-solvent evaporation, J. Magn. Magn. Mater. **311**, 84 (2007).
[26] V. I. Arkhipenko, I. D. Barkov, and V. G. Bashtovoi, Shape of a drop of magnetized fluid in a homogeneous magnetic field, Magnetohydrodynamics **14**, 373 (1979).
[27] J. C. Bacri and D. Salin, Instability of ferrofluid magnetic drops under magnetic field, J. Phys. Lett. **43**, 649 (1982).
[28] M. D. Cowley and R. E. Rosensweig, The interfacial stability of a ferromagnetic fluid, J. Fluid Mech. **30**, 671 (1967).
[29] A. G. Boudouvis, J. L. Puchalla, L. E. Scriven, and R. E. Rosensweig, Normal field instability and patterns in pools of ferrofluid, J. Magn. Magn. Mater. **65**, 307 (1987).
[30] H. Li, T. C. Halsey, and A. Lobkovsky, Singular shape of a fluid drop in an electric or magnetic field, Europhys. Lett. **27**, 575 (1994).
[31] A. Ramos and A. Castellanos, Conical points in liquid-liquid interfaces subjected to electric fields, Phys. Lett. A **184**, 268 (1994).
[32] H. A. Stone, J. R. Lister, and M. P. Brenner, Drops with conical ends in electric and magnetic fields, Proc. R. Soc. A **455**, 329 (1999).
[33] O. E. Séro-Guillaume, D. Zouaoui, D. Bernardin, and J. P. Brancher, The shape of a magnetic liquid drop, J. Fluid Mech. **241**, 215 (1992).
[34] O. Lavrova, G. Matthies, V. Polevikov, and L. Tobiska, Numerical modeling of the equilibrium shapes of a ferrofluid drop in an external magnetic field, Proc. Appl. Math. Mech. **4**, 704 (2004).
[35] S. Afkhami, A. J. Tyler, Y. Renardy, T. G. St. Pierre, R. C. Woodward, and J. S. Riffle, Deformation of a hydrophobic ferrofluid droplet suspended in a viscous medium under uniform magnetic fields, J. Fluid Mech. **663**, 358 (2010).
[36] G.-P. Zhu, N.-T. Nguyen, R. V. Ramanujan, and X.-Y. Huang, Nonlinear deformation of a ferrofluid droplet in a uniform magnetic field, Langmuir **27**, 14834 (2011).

[37] M. S. Korlie, A. Mukherjee, B. G. Nita, J. G. Stevens, A. D. Trubatch, and P. Yecko, Modeling bubbles and droplets in magnetic fluids, J. Phys.: Condens. Matter **20**, 204143 (2008).
[38] J. Zeleny, Instability of electrified liquid surfaces, Phys. Rev. **10**, 1 (1917).
[39] C. T. R. Wilson and G. I. Taylor, The bursting of soap-bubbles in a uniform electric field, Math. Proc. Cambridge Philos. Soc. **22**, 728 (1925).
[40] G. Taylor, Disintegration of water drops in an electric field, Proc. R. Soc. London Ser. A **280**, 383 (1964).
[41] N. M. Zubarev, Formation of conic cusps at the surface of liquid metal in electric field, JETP Lett. **73**, 544 (2001).
[42] N. M. Zubarev, Self-similar solutions for conic cusps formation at the surface of dielectric liquids in electric field, Phys. Rev. E **65**, 055301 (2002).
[43] R. T. Collins, J. J. Jones, M. T. Harris, and O. A. Basaran, Electrohydrodynamic tip streaming and emission of charged drops from liquid cones, Nat. Phys. **4**, 149 (2008).
[44] R. T. Collins, K. Sambath, M. T. Harris, and O. A. Basaran, Universal scaling laws for the disintegration of electrified drops, Proc. Natl. Acad. Sci. USA **110**, 4905 (2013).
[45] S. Neveu-Prin, V. Cabuil, R. Massart, P. Escaffre, and J. Dussaud, Encapsulation of magnetic fluids, J. Magn. Magn. Mater. **122**, 42 (1993).
[46] A. G. Boudouvis, J. L. Puchalla, and L. E. Scriven, Magnetohydrostatic equilibria of ferrofluid drops in external magnetic fields, Chem. Eng. Commun. **67**, 129 (1988).
[47] O. A. Basaran and F. K. Wohlhuter, Effect of nonlinear polarization on shapes and stability of pendant and sessile drops in an electric (magnetic) field, J. Fluid Mech. **244**, 1 (1992).
[48] R. Chantrell, J. Popplewell, and S. Charles, Measurements of particle size distribution parameters in ferrofluids, IEEE Trans. Magn. **14**, 975 (1978).
[49] M. Costabel, in *Mathematical and Computational Aspects*, edited by C. A. Brebbia, W. L. Wendland, and G. Kuhn (Springer, Berlin, 1987), pp. 411–420.
[50] W. L. Wendland, in *Finite Element and Boundary Element Techniques from Mathematical and Engineering Point of View*, edited by E. Stein and W. Wendland (Springer, Vienna, 1988), pp. 273–333.
[51] D. N. Arnold and W. L. Wendland, On the asymptotic convergence of collocation methods, Math. Comput. **41**, 349 (1983).
[52] D. N. Arnold and W. L. Wendland, The convergence of spline collocation for strongly elliptic equations on curves, Numer. Math. **47**, 317 (1985).
[53] J. A. Ligget and J. R. Salmon, Cubic spline boundary elements, Int. J. Numer. Methods Eng. **17**, 543 (1981).
[54] O. Lavrova, V. Polevikov, and L. Tobiska, Equilibrium shapes of a ferrofluid drop, Proc. Appl. Math. Mech. **5**, 837 (2005).
[55] O. Lavrova, G. Matthies, T. Mitkova, V. Polevikov, and L. Tobiska, Numerical treatment of free surface problems in ferrohydrodynamics, J. Phys.: Condens. Matter **18**, S2657 (2006).
[56] M. T. Harris and O. A. Basaran, Capillary electrohydrostatics of conducting drops hanging from a nozzle in an electric field, J. Colloid Interface Sci. **161**, 389 (1993).
[57] B. Kornberger, Fade2D Delauney Triangulation library, http://www.geom.at/products/fade2d/ (2016).
[58] L. C. Wrobel, *The Boundary Element Method: Applications in Thermofluids and Acoustics* (Wiley, New York, 1985), Vol. 1.
[59] O. Lavrova, Numerical methods for axisymmetric equilibrium magnetic-fluid shapes, Ph.D. thesis, Otto-von-Guericke University Magdeburg, 2006.
[60] L. J. Gray, L. F. Martha, and A. R. Ingraffea, Hypersingular integrals in boundary element fracture analysis, Int. J. Numer. Methods Eng. **29**, 1135 (1990).
[61] L. J. Gray, J. M. Glaeser, and T. Kaplan, Direct evaluation of hypersingular Galerkin surface integrals, SIAM J. Sci. Comput. **25**, 1534 (2004).
[62] A. Libai and J. G. Simmonds, *The Nonlinear Theory of Elastic Shells* (Cambridge University Press, Cambridge, 1998).
[63] C. Pozrikidis, *Modeling and Simulation of Capsules and Biological Cells* (Chapman and Hall/CRC, Boca Raton, 2003).

[64] B. Davidovitch, R. D. Schroll, D. Vella, M. Adda-Bedia, and E. A. Cerda, Prototypical model for tensional wrinkling in thin sheets, Proc. Natl. Acad. Sci. USA **108**, 18227 (2011).
[65] R. A. Brown and L. E. Scriven, The shape and stability of rotating liquid drops, Proc. R. Soc. London Ser. A **371**, 331 (1980).
[66] R. Suryo and O. A. Basaran, Local dynamics during pinch-off of liquid threads of power law fluids: Scaling analysis and self-similarity, J. Non-Newton. Fluid Mech. **138**, 134 (2006).
[67] C. R. Anthony, P. M. Kamat, S. S. Thete, J. P. Munro, J. R. Lister, M. T. Harris, and O. A. Basaran, Scaling laws and dynamics of bubble coalescence, Phys. Rev. Fluids **2**, 083601 (2017).
[68] K. N. Christodoulou and L. E. Scriven, Discretization of free surface flows and other moving boundary problems, J. Comput. Phys. **99**, 39 (1992).
[69] E. Zwar, A. Kemna, L. Richter, P. Degen, and H. Rehage, Production, deformation and mechanical investigation of magnetic alginate capsules, J. Phys.: Condens. Matter **30**, 085101 (2018).
[70] J. A. Stratton, *Electromagnetic Theory* (McGraw-Hill, New York, 1941).
[71] S. Ramanujan, Modular equations and approximations to π, Q. J. Math. **45**, 350 (1914).
[72] F. K. Wohlhuter and O. A. Basaran, Shapes and stability of pendant and sessile dielectric drops in an electric field, J. Fluid Mech. **235**, 481 (1992).
[73] T. A. Witten, Stress focusing in elastic sheets, Rev. Mod. Phys. **79**, 643 (2007).
[74] M. Ben Amar and Y. Pomeau, Crumpled paper, Proc. R. Soc. A **453**, 729 (1997).
[75] E. Cerda and L. Mahadevan, Conical Surfaces and Crescent Singularities in Crumpled Sheets, Phys. Rev. Lett. **80**, 2358 (1998).
[76] J.-Y. Sun, X. Zhao, W. R. K. Illeperuma, O. Chaudhuri, K. H. Oh, D. J. Mooney, J. J. Vlassak, and Z. Suo, Highly stretchable and tough hydrogels, Nature (London) **489**, 133 (2012).
[77] V. G. Bashtovoi, S. G. Pogirnitskaya, and A. G. Reks, Determination of the shape of a free drop of magnetic fluid in a uniform magnetic field, Magnetohydrodynamics **23**, 248 (1987).
[78] R. Mercadé-Prieto, R. Allen, Z. Zhang, D. York, J. A. Preece, and T. E. Goodwin, Failure of elastic-plastic core-shell microcapsules under compression, AIChE J. **58**, 2674 (2012).
[79] J. Hegemann, S. Knoche, S. Egger, M. Kott, S. Demand, A. Unverfehrt, H. Rehage, and J. Kierfeld, Pendant capsule elastometry, J. Colloid Interface Sci. **513**, 549 (2018).
[80] L. D. Landau and E. M. Lifshitz, *Theory of Elasticity* (Pergamon, Oxford, 1970).